DMD Fast Forward. Published on July 6, 2015 as DOI: 10.1124/dmd.114.062745
This article has not been copyedited and formatted. The final version may differ from this version.

Title Page

Brain Exposure of Two Selective Dual CDK4 and CDK6 Inhibitors and the Antitumor Activity of CDK4 and 6 Inhibition in Combination with Temozolomide in an Intracranial Glioblastoma Xenograft

Drug Disposition, Lilly Research Laboratories, Eli Lilly and Company, Indianapolis, IN (Thomas J. Raub, Graham N. Wishart, Palaniappan Kulanthaivel, Brian A. Staton, Rose T. Ajamie, Geri A. Sawada), Division of Cancer Research, Eli Lilly and Company, Indianapolis, IN (Lawrence M. Gelbert, Harlan E. Shannon), Discovery Chemistry Research and Technologies, Eli Lilly and Company, Alcobendas (Madrid), Spain (Concepcion Sanchez-Martinez), Covance Laboratories, Greenfield IN (Harlan E. Shannon), Discovery Chemistry Research and Technologies, Eli Lilly and Company, Indianapolis, IN (Alfonso De Dios)

DMD Fast Forward. Published on July 6, 2015 as DOI: 10.1124/dmd.114.062745
This article has not been copyedited and formatted. The final version may differ from this version.

Running Title Page

Running title: CDK4 and CDK6 inhibitor abemaciclib crosses the blood-brain barrier

Corresponding Author: Thomas J. Raub, Ph.D., Drug Disposition, Eli Lilly and Company, Indianapolis, IN 46285; Tel: (317)651-2330; Fax: (317)433-2473; Email: raubtj@lilly.com

Text pages: body of manuscript: 27

Tables: 7

Figures: 7

References: 68

Abstract: 298 words

Introduction: 750 words

Discussion: 2,395 words

Supplement: 2 Tables, 1 Figure

Nonstandard Abbreviations

apical-to-basal	A-B
ATP-binding cassette	ABC
basal-to-apical	B-A
blood-brain barrier	BBB
breast cancer resistance protein	BCRP; ABCG2 (upper case for human)
blood-tumor barrier	BTB
CDK4 and CDK6 kinases	CDK4/6
time zero	D_0

DMD Fast Forward. Published on July 6, 2015 as DOI: 10.1124/dmd.114.062745
This article has not been copyedited and formatted. The final version may differ from this version.

efflux ratio	ER
fetal bovine serum	FBS
fraction unbound	f_u
knockout	KO
liquid chromatography–tandem mass spectrometry	LC-MS/MS
abemaciclib	LY2835219
Mouse Brain Uptake Assay	MBUA
Net efflux ratio	NER
apparent permeability coefficients	P_{app}
P-glycoprotein	P-gp; ABCB1 or MDR1 (upper case for human)
passive permeability coefficients	P_{pass}
retinoblastoma protein	Rb
relative fluorescence units	RFU
Sprague-Dawley	SD
selected reaction monitoring	SRM
time to reach maximum brain concentration	Tmax
Target Engagement Ratio	TER
temozolomide	TMZ
volume of distribution	Vd,ss

DMD Fast Forward. Published on July 6, 2015 as DOI: 10.1124/dmd.114.062745
This article has not been copyedited and formatted. The final version may differ from this version.

ABSTRACT

Effective treatments for primary brain tumors and brain metastases represent a major unmet medical need. Targeting the CDK4/6-cyclin D1-Rb-p16/ink4a pathway using a potent CDK4 and CDK6 kinase inhibitor has potential for treating primary CNS tumors such as glioblastoma and some peripheral tumors with high incidence of brain metastases. We compared CNS exposures of two orally bioavailable CDK4 and CDK6 inhibitors: abemaciclib that is currently in advanced clinical development and palbociclib (IBRANCE®, Pfizer), which was recently approved by the U.S. Food and Drug Administration. Abemaciclib antitumor activity was assessed in subcutaneous and orthotopic glioma models alone and in combination with standard of care temozolomide (TMZ). Both inhibitors were substrates for xenobiotic efflux transporters P-glycoprotein and breast cancer resistant protein expressed at the blood-brain barrier (BBB). Brain $K_{p,uu}$ values were less than 0.2 after equimolar intravenous dose indicative of active efflux, but were ~10 fold greater for abemaciclib than palbociclib. $K_{p,uu}$ increased 2.8 and 21 fold, respectively, when similarly dosed in P-gp-deficient mice. Abemaciclib had a brain AUC(0-24 h) $K_{p,uu}$ of 0.03 in mice and 0.11 in rats following a 30 mg/kg PO dose. Orally-dosed abemaciclib significantly increased survival in a rat orthotopic U87MG xenograft model compared to vehicle-treated animals and efficacy coincided with a dose-dependent increase in unbound plasma and brain exposures in excess of the CDK4 and CDK6 Ki values. Abemaciclib increased survival time of intracranial U87MG tumor-bearing rats similar to TMZ and the combination of abemaciclib and TMZ was additive or greater than additive. These data show abemaciclib crosses the BBB and confirm that both CDK4 and CDK6 inhibitors reach unbound brain levels in rodents that are expected to produce enzyme inhibition, but abemaciclib brain levels are reached more efficiently at presumably lower doses than palbociclib and are potentially on target for a longer period of time.

INTRODUCTION

Effective treatments for primary brain tumors and brain metastases represent a major unmet medical need. Glioblastoma is the most common primary brain tumor, and despite improvements in detection and treatment, the five-year survival for patients with glioblastoma is less than 3% (Ohgaki and Kleihues, 2005). Brain metastases occur in approximately 20-40% of all cancer patients, and its incidence is expected to increase with improved therapy of primary tumors (Patchell, 2003; Steeg et al., 2011). More than 100,000 patients per year die with symptomatic intracranial metastases in the US and the estimated number of new cases of brain metastases diagnosed in the US is 170,000 per year (Langer and Mehta, 2005; Motl et al. , 2006). Brain metastases can develop from a variety of different primary tumors, but the frequency is highest for lung, breast and melanoma cancers (Patchell, 2003; Siena et al., 2010). Metastatic brain tumors are the most common type of brain tumor with an annual four-fold greater incidence compared to primary brain tumors (Chamberlain, 2010).

The cell cycle is the process by which mammalian cells regulate proliferation (Malumbres and Barbacid, 2001). The G1 restriction point was originally described by Pardee as the point where cell proliferation becomes independent of mitogens and growth factors (Pardee, 1974), and the normal function of the restriction point is essential for maintaining control of cellular proliferation (Blagosklonny and Pardee, 2002; Ortega et al., 2002). The restriction point is controlled by the retinoblastoma pathway (CDK4/6-cyclin D1-Rb-p16/ink4a). The retinoblastoma protein (Rb) is a tumor suppressor that inhibits proliferation through binding to and suppressing the activity of the E2F family of transcription factors (Dyson, 1998), and the restriction point is controlled by phosphorylation of Rb by the CDK4 and CDK6 kinases (Blagosklonny and Pardee,2002; Lundberg and Weinberg, 1998). The central role of the Rb

DMD Fast Forward. Published on July 6, 2015 as DOI: 10.1124/dmd.114.062745
This article has not been copyedited and formatted. The final version may differ from this version.

pathway in controlling cellular proliferation is highlighted by its frequent dysregulation in human cancer, including glioblastoma and tumors with a high incidence of brain metastases. Genomic analysis has shown the Rb pathway is dysregulated in approximately 78% of glioblastoma (Cancer Genome Atlas Research Network, 2008), including amplification of CDK4 and deletion of p16/ink4a (Reifenberger et al., 1995; Schmidt et al., 1994). A central role of this pathway also has been established in other tumors with a high incidence of brain metastases such as breast cancer, including HER2-positive breast cancer (Landis et al., 2006; Lin et al., 2008; Malumbres and Barbacid, 2006; Yu et al., 2006), lung cancer (Eichler and Loeffler, 2007), and melanoma (Flaherty and Fisher, 2011). The approval of palbociclib (IBRANCE®, Pfizer) by the U.S. Food and Drug Administration (FDA) in 2015 as first-in-class selective dual inhibitor of CDK4 and CDK6 highlights the importance of this pathway for therapeutic intervention in cancer.

The current standard of care for the treatment of brain tumors and metastases includes radiotherapy, surgery and chemotherapy, but the prognosis for patients is still poor (Eichler and Loeffler, 2007). Delivery of anti-tumor drugs to primary and metastatic cancers in the CNS continues to challenge clinical oncologists. This can be attributed to the blood-brain barrier (BBB) in normal tissue as well as unique features of the blood-tumor barrier (BTB). The BBB physically restricts passive diffusion by many oncolytics and expression of ATP-binding cassette (ABC) efflux transporters at the BBB further limits many anti-cancer drugs from efficiently reaching brain tumors at a concentration required for efficacy (Deeken and Loscher, 2007). P-glycoprotein (P-gp; ABCB1 or MDR1) and breast cancer resistance protein (BCRP; ABCG2) are two efflux transporters with substrate promiscuity sometimes towards transport of the same drug molecule (Sharom, 2008; Chu et al., 2013). Numerous studies have shown that P-gp and BCRP work together at the BBB to restrict brain penetration of drugs

DMD Fast Forward. Published on July 6, 2015 as DOI: 10.1124/dmd.114.062745
This article has not been copyedited and formatted. The final version may differ from this version.

(Kodaira et al., 2010; Agarwal et al., 2011a). While the BBB in brain tumors, or the blood-tumor barrier (BTB), can be physically leakier to diffusion of an anti-cancer drug, this mostly increases drug levels in the tumor core and not at the leading margin, or rim region, of a tumor that is advancing into surrounding normal brain tissue (Lee et al., 2009; Agarwal et al., 2011b). Consequently, recent literature emphasizes the need for new chemotherapy agents that can cross the BBB to allow for improved and durable clinical responses.

The objectives of the studies presented here were to compare CNS exposure of two CDK4 and CDK6 inhibitors either currently in advanced clinical development (abemaciclib) or FDA-approved (palbociclib), and to assess the antitumor activity of abemaciclib in subcutaneous and orthotopic glioma models alone and in combination with temozolomide (TMZ).

MATERIALS & METHODS

Chemicals and Reagents

Abemaciclib [5-(4-Ethyl-piperazin-1-ylmethyl)-pyridin-2-yl]-[5-fluoro-4-(7-fluoro-3-isopropyl-2-methyl-3H-benzoimidazol-5-yl)-pyrimidin-2-yl]-amine and palbociclib [6-Acetyl-8-cyclopentyl-5-methyl-2-[[5-(1-piperazinyl)-2-pyridinyl]amino]pyrido[2,3-d]pyrimidin-7(8H)-one] were synthesized and characterized for purity and identity at Lilly Research laboratories (Indianapolis, IN). Data for abemaciclib and palbociclib described herein were obtained using the methanesulfonate salt of each compound (Table 1). Temozolomide (TMZ; CAS No. 85622-93-1) and LSN335894 were obtained from the Lilly Compound Collection. LSN335984 [(R)-4-[(1a,6,10b)-1,1-dichloro-1,1a,6,10b-tetrahydrodibenzo[a,e]cyclopropa[c]cyclohepten-6-yl]-[(5-quinolinyloxy)methyl]-1-piperazineethanol]

DMD Fast Forward. Published on July 6, 2015 as DOI: 10.1124/dmd.114.062745
This article has not been copyedited and formatted. The final version may differ from this version.

is structurally related to the P-gp-specific inhibitor LY335979 or zosuquidar [(R)-4-[(1a,6,10b)-1,1-difluoro-1,1a,6,10b-tetrahydrodibenzo[a,e]cyclopropa[c]cyclohepten-6-yl]-[(5-quinolinyloxy)methyl]-1-piperazineethanol] (Dantzig et al., 1999). Dimethylsulfoxide (DMSO; 99.7%), 1,2-propanediol and tetrahydrofuran were purchased from Acros Organics (Thermo Fisher Scientific, Waltham, MA). UV grade methanol and acetonitrile were from Honeywell Burdick & Jackson (Muskegon, MI). All other reagents or materials used herein were purchased from Sigma-Aldrich (St. Louis, MO), excluding all cell culture products that were from Invitrogen Life Technologies (Carlsbad, CA), unless otherwise stated.

In Vitro Studies

Efflux Transporter Substrate Assays

MDCK cells expressing either human MDR1 (or ABCB1) or mouse bcrp1 (or abcg2) were obtained at passage number 12 from Dr. Piet Borst at The Netherlands Cancer Institute (Amsterdam, The Netherlands). Details of the assay including calculation of apparent permeability coefficients (Papp) are described by Desai et al. (2013). For specific inhibition of P-gp, LSN335984 (IC50 = 0.4 µM) was used at 2.5 µM (Tombline et al., 2008), and for specific inhibition of bcrp, Chrysin (IC50 = 2.5 µM) was used at 20 µM (Zhang et al., 2004). Cell monolayers were rinsed and extracted with methanol to achieve mass balance and to measure a buffer/cell distribution defined as %Cell or the fraction of mass that was added to the donor and recovered in the methanol rinse. Quantification of test compound was done using liquid chromatography–tandem mass spectrometry (LC-MS/MS).

Efflux Transporter Inhibition Assays

DMD Fast Forward. Published on July 6, 2015 as DOI: 10.1124/dmd.114.062745
This article has not been copyedited and formatted. The final version may differ from this version.

MDCK-MDR1 or MDCK-bcrp cells were plated at a density of 40,000 cells/well in 96-well, flat-bottom cell culture plates in a growth medium volume of 200 µL, which was replaced on day 3. On day 4, cells were washed once with PBSH, and incubated with test compound in PBSH at 37°C under room atmosphere. For the two-dose inhibition screen, cells were washed once with PBSH and pre-incubated with 80 µL of 5 µM or 25 µM test compound, or a range of concentrations to determine an IC_{50} value, in PBSH at 37°C for 30 min. Incubation solutions were then changed to include 0.5 µg/mL calcein-AM (Invitrogen Life Technologies, Carlsbad, CA), a P-gp substrate, or 1 µM Bodipy-prazosin (Invitrogen Life Technologies, Carlsbad, CA), a bcrp substrate (Robey et al., 2003), and incubated for another 20 min. Intracellular fluorescence was measured on a Cytofluor series 4000 multiwell plate reader (PerSeptive Biosystems, Framingham, MA) with λ_{ex} and λ_{em} set to 485 and 530 nm for calcein and for Bodipy-prazosin. Percent inhibition was determined for each test compound by comparing relative fluorescence units (RFU) to that of cells inhibited 100% with either 2.5 µM LSN335984 for P-gp or 20 µM chrysin for bcrp. IC_{50} values were calculated using GraphPad Prism version 4.03 (GraphPad Software, Inc., La Jolla, CA). Briefly, the compound concentration was plotted as log micromolar concentration versus RFU, and a nonlinear dose-response analysis was applied without any special weighting (i.e., assume constant variance) or constraints on the parameter estimates.

Determination of Plasma Protein and Brain Binding

The extent of protein binding was determined in vitro by equilibrium dialysis using a HTDialysis 96-well, 150-µL half-cell capacity, teflon equilibrium dialysis plate and cellulose membranes (12–14 kDa molecular weight cutoff) (HTDialysis LLC; Gales Ferry, CT) as described elsewhere (Zamek-Gliszczynski et al., 2012). Either plasma with K_2EDTA as the anticoagulant (Lampire Biological laboratories,

DMD Fast Forward. Published on July 6, 2015 as DOI: 10.1124/dmd.114.062745
This article has not been copyedited and formatted. The final version may differ from this version.

Pipersville, PA), adjusted to pH 7.4 with phosphoric acid immediately prior to use, or mouse or rat brain homogenate was used. Brain homogenate was prepared in 100 mM phosphate buffer (1:3, w/v; pH 7.4) by probe sonication. Matrices were spiked with DMSO stock solutions of test compounds to give final concentrations of 0.1% DMSO and 1 µM compound. Initial plasma and brain homogenate concentrations were determined by LC–MS/MS as described below. Compound-spiked brain homogenate or plasma were placed into the donor chambers of the dialysis plate (100 µL per half-well), and an equal volume of phosphate buffer (100 mM, pH 7.4) was placed in each corresponding receiver well (n = 3/compound/matrix). The dialysis plate was sealed with the kit adhesive and dialysis was conducted on an orbital shaker (175 rpm) at 37°C for 4.5 h. Following incubation, donor and receiver chamber compound concentrations were determined by LC–MS/MS. Brain homogenate, plasma, and dialysate samples were prepared for bioanalysis by methanol protein precipitation. Fraction unbound (f_u) values were calculated as the ratio of the receiver chamber (buffer) concentration and the donor chamber concentration. Fraction unbound brain was determined by correcting the values in brain homogenate for the three-fold dilution of brain tissue with phosphate buffer (Kalvass and Maurer, 2002). Fraction unbound data were acceptable when compound recovery was 100 ± 30%.

In Vivo Studies

All animal studies were performed in accordance with American Association for Laboratory Animal Care institutional guidelines, and all protocols were approved by the Eli Lilly and Company or Covance Laboratories Animal Care and Use Committee.

Mouse and Rat Brain Uptake Assay

DMD Fast Forward. Published on July 6, 2015 as DOI: 10.1124/dmd.114.062745
This article has not been copyedited and formatted. The final version may differ from this version.

Male CF-1 (normal) or mdr1a(-/-)-deficient CF-1, aka P-gp knockout (KO), mice were obtained from Charles River (Germantown, MD). A simplified, calibrated Mouse Brain Uptake Assay (MBUA) has been described in detail elsewhere (Raub et al., 2006). Mice were acclimated for one week prior to use at 23 ± 1 g bodyweight. Non-fasted mice were dosed intravenously by tail vein injection with 50-µL injectate containing 55 nmole (2.2 µmole/kg) test compound in 8:2 (wt/wt) 1,2-propanediol:DMSO. Alternatively, Sprague-Dawley (SD) rats were dosed intravenously with vehicle or vehicle containing 30 mg/kg LSN335984 one hour before dosing with test compound as described. At 5- and 60-min post-injection, plasma samples, from cardiac blood collected in tubes containing K_2EDTA as the anticoagulant, and excised cerebral hemispheres were immediately frozen and stored at −80°C until bioanalysis. Samples were thawed with 2:1 (v/v for plasma or v/wt for brain) addition of 1:9 (v/v) tetrahydrofuran:acetonitrile and brain samples were homogenized using a Model 100 Sonic Dismembrator (Fisher Scientific, Pittsburqh, PA) prior to removal of precipitated proteins by centrifugation and injection of 1 µL of the supernatant onto the column. Brain concentrations were corrected for an average measured plasma volume of 16 µL/g brain tissue (Raub et al., 2006).

Pharmacokinetic Studies in Rodents

Three female SD rats or twelve female CD-1 mice (Charles River Laboratories, Hollister, CA) were given either a bolus intravenous (IV) dose in 10% (v/v) N-methylpyrrolidone and 18% (v/v) sulfobutyl-7-β-cyclodextrin in 22.5 mM phosphate buffer at pH 3 or an oral (PO) dose in 1% (w/v) hydroxyethylcellulose, 0.25% (v/v) polysorbate 80, and 0.05% (v/v) antifoam in purified water. For the latter, a portion (~20%) of the vehicle was added to the compound and stirred to wet, followed by the remainder of the vehicle. The suspension was probe sonicated on an ice bath to reduce particle size. In

mice, blood samples were obtained by retro-orbital bleed or terminal cardiac puncture while the animals were anesthetized with isoflurane. For pharmacokinetic studies in rats, blood samples (0.15 mL) were withdrawn via an indwelling femoral arterial cannula in rats. In studies in which brain samples were collected, blood was collected by terminal cardiac puncture while animals were anesthetized with isoflurane. Blood samples were collected at the times indicated in tubes containing K_2EDTA as the anticoagulant. Samples were centrifuged within 1 h of collection and plasma was collected and stored at −80°C until analysis. Total concentrations of the compound were determined by LC-MS/MS. Where brain concentration was determined, brains were collected from three different animals at each time point, rinsed with ice-cold saline, weighed, and stored at −80°C until analysis. Brain homogenate concentrations were converted to brain concentrations for the calculations of brain-to-plasma ratios.

Distribution Studies in Rats

The distribution of abemaciclib-related radioactivity was evaluated by quantitative whole-body autoradiography. One animal per time point was administered a single oral dose of 10 mg/kg containing 200 µCi [^{14}C]abemaciclib to SD rats. The dose was formulated in purified water containing 1 M phosphoric acid and administered to rats as a solution. Following drug administration, rats were sacrificed via exsanguination under isoflurane anesthesia at 1, 2, 4, 8, 12, 24, 48, 72, 120, 168, 336, 504, and 672 h post-dose. Blood (at least 5 mL) was collected into tubes containing K_2EDTA. The carcasses were immediately frozen in a hexane/dry ice bath for approximately 10 min. Each carcass was drained, blotted dry, placed into a bag and stored at approximately -70°C for at least 2 h, then stored at -20°C. The frozen carcasses were embedded in chilled carboxymethylcellulose and frozen

DMD Fast Forward. Published on July 6, 2015 as DOI: 10.1124/dmd.114.062745
This article has not been copyedited and formatted. The final version may differ from this version.

into blocks. Prior to section collection, standards fortified with ^{14}C radioactivity were placed into the frozen block containing the carcass and were used for monitoring the uniformity of section thickness. Appropriate sections were collected on adhesive tape at 40-µm thickness using a Leica CM 3600 cryomicrotome. Sections were collected at five to eight levels of interest in the sagittal plane for analysis. The mounted sections were tightly wrapped with Mylar film and exposed on phosphor imaging screen along with fortified standards for subsequent calibration of the image. After 4 days of exposure, screens were scanned using an Amersham Biosciences Strom scanner. The standard image data were analyzed using Imaging Research Inc. AIS software to create a calibrated standard curve. Tissue concentrations were then interpolated from each standard curve as nCi/g and then converted to ng equivalents (ng·eq)/g on the basis of the test article specific activity. Pharmacokinetic parameters including maximum concentration (C_{max}) and area under the concentration-time curve from time 0 to the last measurable time point (AUC_{0-t}) were calculated by using WinNonlin Professional Edition, version 5.2 (Pharsight Corporation, Cary, NC).

LC-MS/MS Analysis

All compound concentrations were determined with LC-MS/MS assays developed at Lilly using precursor and product ions specific to each compound. Plasma samples and standards were de-proteinated with acetonitrile/tetrahydrofuran (9:1, v/v) or acetonitrile/methanol (1:1, v/v). Brain samples were extracted with acetonitrile/tetrahydrofuran (9:1, v/v) or homogenized with methanol/water (1:4, v/v) then mixed with acetonitrile/methanol (1:1, v/v) to precipitate proteins. Fractions of the resulting supernatants were then submitted to LC-MS/MS analysis. Temozolomide was measured by selected reaction monitoring (SRM) in positive ion mode (m/z transition of

DMD Fast Forward. Published on July 6, 2015 as DOI: 10.1124/dmd.114.062745
This article has not been copyedited and formatted. The final version may differ from this version.

195.1>137.9) with a Polar RP 2 x 100 mm, 5 micron column (Phenomenex, Torrance, California) and a 10 mM ammonium acetate mobile phase eluted with a methanol gradient. Palbociclib was measured by SRM in positive ion mode (m/z transition of 448.2>380.2) with either an XTerra MS-C8 2.1 x 100 mm, 5 micron column (Waters Corp, Milford, Massachusetts) or a Polar RP 2 x 100 mm, 5 micron column, and a 5 mM formic acid mobile phase eluted with a methanol gradient. Abemaciclib was measured by SRM in positive ion mode (m/z transition of 507.3>393.1) with either a Polar RP 2 x 100 mm 5 micron column and a 5 mM formic acid mobile phase eluted with a methanol gradient, or a Betasil C18 2 × 20 mm 5 micron Javelin column (Thermo Scientific, Waltham, Massachusetts) using either a 5 mM ammonium bicarbonate mobile phase and methanol gradient, or a 0.4% TFA/1mM ammonium bicarbonate mobile phase and acetonitrile gradient. All mass spectrometric detection was performed with an API 4000 (Applied Biosystems, Foster City, California) mass spectrometer equipped with a TurboIonSpray® source and tuned to achieve unit resolution (0.7 DA at 50% FWHM). Data were acquired and processed with Analyst 1.4.2 (Applied Biosystems).

In Vivo Xenograft Studies

U87MG glioblastoma cells were obtained from American Type Culture Collection and maintained using the recommended culture conditions. Cell line authenticity was confirmed by DNA fingerprinting (IDEXX BioResearch, Columbia, MO).

For subcutaneous xenograft studies, cells were harvested and resuspended in a 1:1 mixture of serum-free media and Matrigel (BD Biosciences, San Jose, CA), and 5 x 10^6 cells were injected subcutaneously into the rear flank of 5-to-6-week-old CD1 nu/nu female mice (Harlan Laboratories). Tumor volume

was estimated by using the formula: volume = l x w^2 x 0.536, where l and w are measured perpendicular diameters, and l is greater than or equal to w.

When the mean tumor volume was approximately 150 to 300 mm^3, animals were randomized to treatment groups by tumor volume. Abemaciclib was formulated in 1% hydroxyethyl cellulose and 0.1 % antifoam in 25 mM phosphate buffer pH 2 and administered orally by gavage (final volume 0.2 mL) at the indicated dose and schedule. Temozolomide was formulated in distilled water containing 1% Carboxymethyl cellulose and 0.25% Tween-80 and administered by intraperitoneal injection. Tumor volume and body weight were measured twice weekly. For analysis, tumor volume data were transformed to a log scale to equalize variance across time and treatment groups. The log volume data were analyzed with a two-way repeated measures analysis of variance by time and treatment using the MIXED procedure in SAS software (version 9.2). The spatial power law covariance structure, SP(POW) option, was utilized to account for unequal longitudinal spacing of the volume measurements. Treated groups are compared to the control group at each time point. Treated groups are compared to the control group at each time point.

The orthotopic xenograft studies were performed similarly as described elsewhere (Agarwal et al., 2013) with 5 x 10^5 cells implanted. The animals were randomized to treatment groups four days after tumor implantation (8 animals per group). The primary outcome variable was survival. Animals were monitored daily until death and, in consultation with the veterinary staff and in adherence with the policy on tumor implantation, euthanized if the animal became moribund. Data analysis was performed using JMP software (SAS Institute) and a log-rank test.

RESULTS

Transport studies in transfected cell lines

The bidirectional transport of abemaciclib and palbociclib was assessed in MDCK cell lines overexpressing human P-gp or mouse bcrp (Tables 2 and 3). The mean apparent passive permeability coefficients (P_{pass}) measured in the presence of LSN335984, a specific inhibitor of P-gp, were slow (abemaciclib) and moderate (palbociclib) at 18 nm/sec and 180 nm/sec, respectively. However, the P_{pass} values for both compounds were most likely under-measured because of their propensity to partition into the cell monolayer as indicated by the recovery of 56% and 32%, respectively, of the total mass added and recovered in the methanol wash, e.g., %Cell (Table 2). The range of P_{pass} values measured in this assay was from 5 to 700 nm/sec (Sawada G, data not shown). In the absence of P-gp inhibition, both compounds had NERs of 4.6 (abemaciclib) and 9.2 (palbociclib) indicating both were substrates for P-gp (Table 2). Inhibition of P-gp with LSN335984 decreased the ER values to 0.8 and 1.4, respectively, as expected for loss of net efflux in this assay. Chrysin, an inhibitor of bcrp, had no effect (data not shown). The %Cell for both compounds also decreased with P-gp inhibition, but only by 18% (abemaciclib) and 30% (palbociclib) due to their apparently high cell partitioning. Inhibition of P-gp activity by 5 µM of each compound, equivalent to the concentration used in the flux experiment, was measured as a percent decrease in transport of the P-gp substrate Calcein-AM relative to the LSN335984 (Table 2). Abemaciclib inhibited P-gp activity by 30% relative to 100% inhibition by LSN335984 whereas palbociclib had minimal effect at up to 25 µM.

In the absence of bcrp inhibition, both compounds had NERs of 9 (abemaciclib) and 11 (palbociclib) indicating both are substrates for bcrp in vitro (Table 3). Inhibition of bcrp with chrysin decreased the

ERs to 1.2 and 1.5, respectively, as expected for loss of net efflux in this assay. LSN335984, which is an inhibitor of P-gp, had no effect (data not shown). The %Cell for palbociclib also decreased 82% with bcrp inhibition, but abemaciclib %Cell did not change. Inhibition of bcrp activity by 5 µM of each compound, equivalent to the concentration used in the flux experiment, was measured as a percent decrease in transport of the bcrp substrate Bodipy-prazosin relative to the chrysin (Table 3). Abemaciclib and palbociclib similarly inhibited bcrp activity by 21-29% at 5 µM relative to assumed 100% inhibition by chrysin.

Plasma protein and brain tissue binding

Binding of abemaciclib and palbociclib to plasma proteins was 95-98% and ~78%, respectively, for at least two animal species, but palbociclib was ~5-fold less bound than abemaciclib in plasma at 1 µM (Table 4). Binding to brain tissue was greater for both compounds, but ~2.5- to 6-fold less for palbociclib versus abemaciclib albeit within the 3- to 4-fold variability characteristic of the assay (Table 4). These unbound fraction values were used in calculations of unbound exposures obtained for rodent pharmacokinetic and efficacy studies.

Pharmacokinetics in mice

The unbound plasma and brain concentrations versus time profiles of abemaciclib following a single PO administration of 30 mg/kg to mice are presented in Figure 1. Oral absorption was fast and the time to reach maximum brain concentration (T_{max}) was 2 h (Table 5). Abemaciclib free brain concentrations between 0.5 and 24 h were 26 ± 14-fold the mean CDK4/cyclinD1 K_i^{ATP} of 0.6 nM and 6 ± 3-fold the CDK6/cyclinD1 K_i^{ATP} of 2.4 nM (Gelbert et al., 2014), suggesting that abemaciclib would be able to

DMD Fast Forward. Published on July 6, 2015 as DOI: 10.1124/dmd.114.062745
This article has not been copyedited and formatted. The final version may differ from this version.

modulate the CDK4 and CDK6 pathway in the brain at this dose. The $K_{p,brain}$ (AUC or C_{max}) remained unchanged and was 0.21 ± 0.04 over 24-h post-dose. The unbound brain-to-unbound plasma concentration ratio or $K_{p,uu}$ was 0.03 ± 0.01 consistent with active efflux limiting brain exposure (Hammarlund-Udenaes et al., 2008) (Table 5).

In a separate study, abemaciclib and palbociclib were dosed intravenously (bolus) at 0.5, 2.2, 5.4, and 10.9 µmole/kg in the MBUA using normal CF-1 mice and the 5-min plasma and brain levels were measured. Plasma exposures for both compounds were proportional to dose (Supplement Table 1A). Likewise, brain exposures for both compounds were proportional to dose (Supplement Table 1A). However, Figure 2 shows the nonlinear relationship between $K_{p,brain}$ and plasma concentration for abemaciclib indicative of saturation of efflux transport. $K_{p,brain}$ increased from 0.37 to 2.9, which compared to the $K_{p,brain}$ measured in P-gp KO mice (Table 6; Supplement Table 1A). $K_{p,uu,brain}$ increased from 0.04 to 0.48 (Supplement Table 1B). Apparently, the exposures of palbociclib were too low to achieve saturation at the doses used, where $K_{p,brain}$ was ~0.14 except for the highest dose, but all were well below the $K_{p,brain}$ of 2.4 in P-gp KO mice (Table 6; Supplement Table 1A). The total and unbound EC_{50} values for palbociclib estimated from the plot were 8.5 µM and 1.5 µM, respectively. These values are approximations given the extrapolation of the minimally defined, dose response curve. The total and unbound EC_{50} values for abemaciclib were 1.8 µM and 95 nM, respectively. Thus, this suggests that abemaciclib more readily (~16-fold) saturated the BBB efflux transport resulting in greater brain exposure for abemaciclib at equivalent doses of palbociclib. We called this the BBB P-gp EC_{50} that assumes the unbound fraction (measured at a total concentration of 1 µM) is not changing within this range of total concentrations (up to 13 µM) and ignores that net exposure may be greater after the bolus IV dose (Padowski and Pollack, 2011).

Exposure in Efflux Transporter Knockout Mice

Abemaciclib or palbociclib were dosed IV (bolus) in the MBUA using male normal CF-1 or P-gp KO mice at 2.2 µmole/kg (~1.2 mg/kg) (Table 6). Total brain exposure of palbociclib increased 16-43 fold in P-gp KO mice compared to normal mice at 5 and 60 min post-dose (Supplement Table 2). In contrast, abemaciclib appears to penetrate the BBB of normal mice more effectively (~12-fold) despite it also being an efflux transporter substrate. Moreover, total brain exposure of abemaciclib only increased 3-7 fold in P-gp KO mice implying that abemaciclib is a less efficient P-gp substrate.

Table 6 compares the unbound plasma and brain exposures in these experiments. Despite 4.2-fold greater unbound plasma levels for palbociclib in mice, abemaciclib reached ~3-fold greater unbound brain levels in normal mice. This is explained by the differential effect of efflux transport on each compound and the differences in unbound fractions. The $K_{p,brain}$ in normal mice was 1.2 for abemaciclib and 0.1 for palbociclib, and deletion of P-gp in the KO mice resulted in similar $K_{p,brain}$ values of 3.2 and 2.3, respectively. However, accounting for the unbound fractions and calculating $K_{p,uu,brain}$ clearly showed that abemaciclib was ~17-fold more effective at equilibrating with the brain than palbociclib under these conditions and exposures after equimolar intravenous doses. There was no indication in these studies that systemic clearance of either compound is dependent upon P-gp because the relative decrease in total plasma levels from 5 min to 60 min in normal versus P-gp KO mice were comparable (Supplement Table 2). Abemaciclib had a loss in plasma levels of 67 ± 4% in normal mice and 78 ± 4% in P-gp KO mice. Palbociclib had a loss of 55 ± 8% in normal mice and 68 ± 5% in P-gp KO mice. In contrast, loss of both compounds from the brain was delayed by deletion of P-gp. Abemaciclib had a loss in brain levels of 53 ± 15% in normal mice and 26 ± 15% in P-gp KO mice, and palbociclib had a loss

DMD Fast Forward. Published on July 6, 2015 as DOI: 10.1124/dmd.114.062745
This article has not been copyedited and formatted. The final version may differ from this version.

of 36 ± 4% in normal mice and 0% in P-gp KO mice where brain levels appeared to be increasing at 60 min versus 5 min (Supplement Table 2). In a separate study, the plasma AUC(0-8 h) of abemaciclib was shown to be increased less than 2-fold after PO dosing 10 mg/kg in FVB mdr1a/1b(-/-) and bcrp(-/-) KO mice (Taconic Farms, NY) compared to FVB control (data not shown); however, corresponding brain levels were not measured.

Pharmacokinetics in rats

The unbound plasma and brain concentrations versus time profiles of abemaciclib and palbociclib following a single PO administration of 30 mg/kg to rats are shown in Figure 3. Oral absorption of abemaciclib was slow with a brain T_{max} of 4 h (Table 5). Abemaciclib free brain concentrations between 2 and 48 h were 14 ± 5-fold the mean CDK4/cyclinD1 K_i^{ATP} of 0.6 nM and 3.5 ± 1.3-fold the CDK6/cyclinD1 K_i^{ATP} of 2.4 nM, suggesting that abemaciclib should be able to modulate the CDK4 and CDK6 pathway in the brain at this dose. The AUC and C_{max} $K_{p,brain}$ values were similar and $K_{p,brain}$ remained unchanged at 0.86 ± 0.14 over 48 h post-dose. $K_{p,uu,brain}$ was 0.10 ± 0.02 consistent with active efflux limiting brain exposure (Table 5). Unbound plasma concentrations of abemaciclib were approximately equal to the in vivo mouse BBB P-gp EC_{50} of 95 nM suggesting that P-gp might be partially saturated at 30 mk/kg PO. Based upon these data and increased exposures observed with increasing dose up to a PO dose of 100 mg/kg, abemaciclib was dosed at 20, 40, and 80 mg/kg for the intracranial xenograft experiments discussed below.

A CDK4/cyclinD1 K_i^{ATP} of 2.9 nM and a CDK6/cyclinD1 K_i^{ATP} of 1.4 nM were similarly measured for palbociclib (Torres, R., unpublished data). Using the brain exposures measured in the rat PK study, palbociclib free brain concentrations were 6.3 ± 0.2-fold its measured CDK4 K_i and 2.9 ± 1.9-fold its

DMD Fast Forward. Published on July 6, 2015 as DOI: 10.1124/dmd.114.062745
This article has not been copyedited and formatted. The final version may differ from this version.

measured CDK6 K_i for up to 4 h, suggesting that palbociclib should be able to modulate the CDK4 pathway in the brain. However, unlike abemaciclib the palbociclib brain and plasma levels decreased with time resulting in unbound levels (Figure 3) that were markedly less than the CDK4 and CDK6 K_i values. The AUC $K_{p,brain}$ was 0.17 and $K_{p,uu}$ was 0.02 ± 0.01 over time consistent with active efflux limiting brain exposure.

Brain Exposure in Rats Co-dosed with P-gp Inhibitor

The brain exposures of abemaciclib and palbociclib also were compared using SD rats in an experimental design identical to the MBUA described above. Instead of using P-gp-deficient rats that were not yet available at the time, we dosed rats intravenously with 30 mg/kg LSN335984 (specific P-gp inhibitor) at one hour before dosing with test compound at 2.2 μmole/kg. Similar to mice, BBB penetration of palbociclib was markedly limited by P-gp efflux whereas abemaciclib was less so (Table 7; Supplement Table 2). Accounting for the unbound fractions to calculate $K_{p,uu,brain}$, abemaciclib is ~9-fold more effective at crossing the BBB than palbociclib under these conditions and systemic exposures after equimolar doses. As with P-gp knockout mice, there was no indication in these studies that systemic clearance of either compound is dependent upon P-gp or influenced by pre-treating with LSN335984 (Supplement Table 2).

Regional Brain Exposure of Abemaciclib in Rats

Following a single oral dose of 10 mg/kg of [^{14}C] abemaciclib to rats, drug-related radioactivity was extensively distributed into tissues and organs. Radioactivity concentrations in CNS tissues, cerebellum, cerebrum, medulla, and olfactory lobe, were measurable up to 12 h. Radioactivity

DMD Fast Forward. Published on July 6, 2015 as DOI: 10.1124/dmd.114.062745
This article has not been copyedited and formatted. The final version may differ from this version.

concentrations in choroid plexus were measurable up to 72 to 336 h. Radioactivity exposure (AUC_{0-t}) in these tissues relative to plasma exposure is shown in Figure 4. Except for choroid plexus, the tissue-to-plasma ratios (K_p) based on AUC and C_{max} for the CNS regions ranged from 0.12 to 0.45 and 0.26 to 0.79, respectively, with highest ratios observed for cerebrum. It was determined that 80% of the plasma radioactivity represented parent abemciclib.

Efficacy in a brain tumor model

Abemaciclib has been shown previously to have in vitro and in vivo antitumor activity against subcutaneous human xenograft tumors of diverse histologic origin, including lung, breast and melanoma representing human cancers that frequently metastasize to the brain (Dempsey et al., 2013; Gelbert et al., 2014). In the present study, we used both subcutaneous and orthotopic glioblastoma U87MG xenografts to assess the antitumor activity of abemaciclib alone or when combined with TMZ. Figure 5A shows the dose-dependent increase in survival in a rat orthotopic U87MG xenograft study with abemaciclib when compared to vehicle-treated animals, where the 40-mg/kg and 80-mg/kg doses significantly increased survival by 7.5 ± 1.3 days ($p = 0.032$) and 10 ± 1.3 days ($p = 0.0006$), respectively. No animals were lost in the groups treated with abemaciclib during the treatment period (days 4-25), suggesting tumor growth was inhibited during treatment. Consistent with the survival data, a dose-dependent increase in both total and unbound plasma and brain exposure was observed (Figure 5B). Only the 40- and 80-mg/kg dose groups showed unbound brain levels in excess of both the CDK4 and CDK6 Ki values.

Temozolomide is an alkylating agent approved for the treatment of glioblastoma, and the effect of combining abemaciclib with TMZ was assessed first in mouse subcutaneous U87MG glioblastoma

DMD Fast Forward. Published on July 6, 2015 as DOI: 10.1124/dmd.114.062745
This article has not been copyedited and formatted. The final version may differ from this version.

xenografts. Abemaciclib at 50 mg/kg or 3 mg/kg TMZ alone had a similar inhibition of xenograft growth, and the combination gave a greater inhibition of tumor growth than either individual treatment (Figure 6). Comparison of changes in body weight for all groups showed little effect of the treatments on body weight, indicating the combination treatment was well tolerated (data not shown).

The combination of abemaciclib and TMZ was then assessed using the rat U87MG orthotopic model. Abemaciclib (40 mg/kg) or TMZ (3 mg/kg) alone were efficacious as either treatment significantly increased survival by 9 and 16.5 days, respectively, when compared to the vehicle-treated group (Figure 7). The combination of abemaciclib (40 mg/kg) and TMZ (3 mg/kg) had an additive or greater than additive effect on survival when compared to the survival benefit of the individual treatments alone where survival was increased by 31 to 37.5 days (relative to untreated control) depending upon the dosing schedule (Figure 7).

DISCUSSION

Targeting the CDK4/6-cyclin D1-Rb-p16/ink4a pathway through the discovery of potent CDK4 and CDK6 kinase inhibitors has potential for treating primary CNS tumors such as glioblastoma and certain peripheral tumors with a high incidence of brain metastases. The G1 restriction point is critical for regulating the cell cycle and is controlled by the CDK4 and CDK6 kinases and their associated pathway. Abemaciclib or palbociclib specifically inhibits CDK4 and 6, thereby inhibiting Rb protein phosphorylation in early G1. This prevents CDK-mediated G1-S phase transition, which arrests the cell cycle, suppressing DNA synthesis and inhibiting cancer cell growth.

The clinical responsiveness of brain tumors to standard chemotherapy and molecularly targeted drugs are “unambiguously disappointing” (Steeg et al., 2011). Despite the high frequency of metastatic brain tumors, there is no accepted paradigm for treatment with chemotherapy (Gerstner and Fine, 2007). The BBB restricts the diffusion of many drugs into the brain inclusive of limiting highly permeable drugs by active efflux transporters expressed at the BBB and the BTB. In contrast, the BTB is assumed by many clinicians to be leaky as suggested by the diffusion of contrast agents for computed tomography or magnetic resonance imaging into tumors. However, researchers are calling this a misconception as evidenced by the low tumor concentrations for most chemotherapeutic agents in brain tumors and the poor clinical outcomes (Vogelbaum and Thomas, 2007). BBB leakiness associated with CNS tumors is typically local and heterogeneous. The compromised barrier occurs in the tumor core, but is fully intact at the growing tumor border. Gliomas are associated with aggressive invasion of the surrounding brain parenchyma (de Vries et al., 2009; Lee et al., 2009). While resection reduces the primary tumor burden, extensive migration of glioma cells away from the primary tumor mass prevents the complete removal of tumor cells (Lee et al., 2009). Thus, after surgical removal of the primary tumor core, these residual tumor cells that infiltrate the normal parenchyma at the tumor border are protected by an intact BBB, and these cells often grow into larger and more aggressive tumors (Agarwal et al., 2011a).

In contrast to primary gliomas, metastatic brain tumors appear to have a more permeable BTB suggesting that metastatic brain tumors could be treated differently than gliomas (Gerstner and Fine, 2007; Fortin, 2012). Studies also suggest lower P-gp expression in the BBB of metastatic brain tumors as compared with gliomas (Gerstner and Fine, 2007). Using an experimental model for brain metastasis, Lockman et al. (2010) demonstrated partial BTB permeability compromise in greater than

DMD Fast Forward. Published on July 6, 2015 as DOI: 10.1124/dmd.114.062745
This article has not been copyedited and formatted. The final version may differ from this version.

89% of experimental metastatic lesions. More importantly, cytotoxic concentrations were reached in only 10% of the most permeable metastases. A similar conclusion was reached for lapatinib and its activity against brain metastases of breast cancer (Taskar et al., 2012). Both studies concluded that the BTB remains a significant impediment to standard chemotherapeutic delivery and efficacy in experimental brain metastases. Given these arguments, the next generation of clinically successful oncolytics must be effectively delivered across the BBB in consideration of treating brain tumors as a disease of the whole brain (Agarwal et al., 2011b).

Unbound brain concentration is the most relevant parameter in assessing the pharmacodynamic response of a CNS agent (Wager et al., 2011). However, it is obvious that abemaciclib and palbociclib do not entirely meet the physicochemical guidelines for optimal unbound exposure of CNS compounds (Wager et al., 2011). Abemaciclib and palbociclib have suitable log octanol-water partition coefficients, but exceed the recommended molecular weight of 305 Da and topological polar surface area of 45 $Å^2$. Greater than 75% of CNS drugs also have good passive permeability and low efflux liability (Wager et al., 2011). Some have gone as far to advise not advancing efflux transporter substrates for CNS targets because of a high risk associated with low confidence in human translation (Di et al., 2013). These non-CNS optimal, physicochemical attributes are not atypical for most of the antitumor drugs developed to date, especially kinase inhibitors.

Abemaciclib and palbociclib are substrates for human P-gp and mouse bcrp; both compounds have restricted BBB penetration that is improved by elimination of P-gp in rodents. However, the efficiency of efflux for abemaciclib appears to be lower than palbociclib as shown by the in vitro efflux ratios of 4.1 and 12, respectively, which align with the greater $K_{p,uu,brain}$ measured for abemaciclib.

Unfortunately, we were unable to assess the in vivo impact of bcrp on brain exposure of these compounds. Numerous studies have shown that P-gp and BCRP work together at the BBB to restrict brain penetration of drugs (Kodaira et al., 2010; Agarwal et al., 2011a). This might be the reason that the $K_{p,uu}$ of neither abemaciclib (0.48; Table 6) nor palbociclib (0.21; Table 6) in P-gp KO mice approached a value of 1.0, indicative of passive diffusion, such that bcrp is still active in these mice. This also was seen in the rat studies pre-dosed with the P-gp-specific inhibitor (Table 7).

Optimizing unbound brain and plasma concentration ratios may increase the probability of conclusively testing the pharmacological hypotheses in clinical studies. Ultimately, enough unbound brain concentration delivered to the target is most important. To monitor scaffold optimization, we used the ratio of the unbound brain concentration to the in vitro enzyme IC_{50} or K_i, that we call the Target Engagement Ratio (TER), as a crude predictor for expectations of efficacy. If the TER is close to or greater than 1.0 for a predetermined period of time, then a 50% or greater inhibition of CDK4 and CDK6 should occur. In these experiments, we have assumed that the inhibitors' potencies at the targets are not different across species. When rats were dosed orally with 30 mg/kg and brain levels measured for 48 h (Fig. 3), both abemaciclib and palbociclib reached unbound brain concentrations of 13 nM and 19 nM, respectively, at 4 h or $C_{max,plasma}$ to give TER values of 21 and 6.5, respectively, for CDK4 inhibition, which primarily reflects their difference in enzyme inhibition potency. However, abemaciclib TER values of >10 for brain were sustained ~40 hours longer than for palbociclib due to its slower intrinsic unbound clearance from rat plasma and brain. Similarly, abemaciclib had sustained brain TER values of 3.3-14.3 for ~12 h in mice dosed with 30 mg/kg. These data suggest that both compounds can reach unbound brain levels that would be expected to produce enzyme inhibition, but that abemaciclib brain levels are more efficiently reached at presumably lower doses than palbociclib

DMD Fast Forward. Published on July 6, 2015 as DOI: 10.1124/dmd.114.062745
This article has not been copyedited and formatted. The final version may differ from this version.

and are most likely on-target longer. The distribution study using radiolabeled abemaciclib indicated that radioactivity is distributed to all regions of the rat brain with highest concentrations observed in cerebrum.

Approximately 78% of gliomas have alterations in the CDK4 and CDK6 pathway, most notably amplification of CDK4, suggesting potential sensitivity to CDK4 and CDK6 inhibitors. Likewise, U87MG cells have a homozygous deletion of p16/ink4a that also occurs in 52% of primary human tumors, including lung and breast. Loss of p16/ink4a results in activation of the CDK4 pathway (Parsons et al., 2008). U87MG cells have a high and reproducible tumor take rate and narrow survival window so that tumors can be generated easily for preclinical testing. Moreover, U87MG cells also are null for PTEN, as are ~36% of human GBM, which results in resistance to TMZ (Jiang et al., 2007). Unlike gliomas, orthotopic U87MG tumors have a non-diffusely infiltrative growth pattern with a well-demarcated tumor mass (de Vries et al., 2009; Radaelli et al., 2009; Jacobs et al., 2011). Orthotopic U87MG tumors also have significantly more homogeneous and leaky vessels (de Vries et al., 2009) compared to gliomas, which allows even poorly brain-penetrant compounds to reach the tumor. In one study, 2.3-fold more unbound drug was measured in tumor compared to contralateral, non-tumor-bearing brain (Carcaboso et al., 2010). U87MG tumors also express P-gp and BCRP (Carcaboso et al., 2010) consistent with clinical findings in gliomas (Fattori et al., 2007), but the functional significance of this expression can be questioned. For example, GDC-0941, a P-gp and BCRP substrate, was efficacious in the orthotopic U87MG model reducing tumor volume by >60% despite limited brain penetration in the presence of an intact BBB (Salphati et al., 2012). Some of these criticisms about the translatability of the U87MG model were acknowledged by demonstrating activity in this model, which is typically used as a prerequisite for clinical testing. Abemaciclib as a single treatment was shown here to dose-

dependently increase rat survival in this model. Temozolomide is approved for the treatment of adult patients with newly diagnosed glioblastoma multiforme (Friedman et al., 2000). We also showed here that abemaciclib (40 mg/kg) alone or TMZ (3 mg/kg) alone had similar increases in survival time of intracranial U87MG tumor-bearing rats. These data show that the combination of abemaciclib and TMZ was additive or greater than additive for increased days of survival.

We calculated the brain TER values for CDK4 K_i obtained in the three oral doses of 20, 40, and 80 mg/mL per day for 21 days to be 0.8, 4.2, and 9.9 at 4 h after the last dose (Fig. 5B). This corresponded well to the observed increased survival of tumor-bearing mice where the lowest dose was not significantly efficacious with a brain TER value of <1 and prolonged survival in the two higher dose groups was significant with brain TER values of >1. The same trend was observed for the TER values using CDK6 K_i. Unbound levels of palbociclib were reported in normal brain surrounding the U87MG xenograft tumor and in the contralateral hemisphere of approximately 25-40 nM after 4 weeks at 150 mg/kg per day (Michaud et al., 2010), which is the maximum tolerated dose. This corresponds to estimated brain TER values of 8.6-15 for the CDK4 K_i used herein and is similarly consistent with the observed arrested growth of U87MG cell xenografts and significantly improved survival of tumor-bearing mice.

We also showed that abemaciclib is capable of saturating mouse BBB P-gp efflux with an unbound EC_{50} of 95 nM (Fig. 2), which suggests brain exposure of abemaciclib might be enhanced because of this innate characteristic. But, is it really possible to rescue a P-gp/BCRP substrate for CNS indications using saturation as a clinical strategy for compound design? Others have argued that saturation of P-gp/BCRP at the human BBB is very difficult to achieve clinically for several reasons: the unbound blood

DMD Fast Forward. Published on July 6, 2015 as DOI: 10.1124/dmd.114.062745
This article has not been copyedited and formatted. The final version may differ from this version.

concentration of drug is usually too low even at high doses; efflux transporters are typically of high capacity and low affinity (Kalvass et al., 2013; Di et al., 2013). Yet, BBB efflux transport saturation has been achieved in animal models (Cisternino et al., 2003; Geldof et al., 2008; Polli et al., 2009; Sane et al., 2012). In our case, even though we achieved unbound plasma concentrations (902 nM in mouse; Fig. 1 and 109 nM in rat; Fig. 3) that were greater than the mouse BBB P-gp unbound EC_{50} of 95 nM, we did not observe a marked change in the $K_{p,uu,brain}$ values of 0.03 (mouse) and 0.11 (rat) after oral dosing relative to the $K_{p,uu,brain}$ values obtained with low intravenous doses. This suggests that abemaciclib is unlikely able to predictably increase its own diffusion across the BBB or BTB, or that the 2-fold increase expected at a $C_{u,plasma}/EC_{50}$ ratio of ~1.0 is insignificant. Clinical evidence indicates that drug interactions at the human BBB due to efflux transporter inhibition by marketed drugs are low in magnitude or less than a 2-fold increase in $K_{p,brain}$, e.g., a 50% inhibition (Kalvass et al., 2013). The mean unbound plasma levels for abemaciclib of 15 nM achieved clinically (Shapiro et al., 2013) are markedly less than the mouse BBB EC_{50} of 95 nM, so partial saturation of P-gp is unlikely. We attribute the greater $K_{p,uu,brain}$ values obtained after IV dosing to the much greater unbound plasma concentrations achieved immediately after the bolus dose. In effect, the EC_{50} measured at 5 min is most likely well underestimated. We tried generating a K_i/K_m value for abemaciclib against the human P-gp expressed in MDCK cells, but this failed due to the high buffer-to-cell partitioning of this compound. So, P-gp/BCRP substrate saturation as a strategy for improving CNS indications is not tenable for an orally dosed compound.

Phase I mean plasma C_{max} exposures were reported for palbociclib of 97 ng/mL or 217 nM after dosing 21 days at 125 mg once daily (Flaherty et al., 2012). If we assume that binding in human plasma is similar to mouse and rat, e.g., $f_{u,plasma}$ of 0.22, then using the $K_{p,uu,brain}$ value measured in rat predicts a

human brain unbound exposure of approximately 0.7 nM, which is lower than the K_i values of 1.4-2.9 nM for CDK4 and 6. This estimated unbound brain exposure is similar when the observed $K_{p,brain}$ of 0.1 in rat and mouse and the measured rat $f_{u,brain}$ of 0.027 are used for the calculation. In a phase I study in advanced cancer patients (n =22), a mean plasma $C_{max,ss}$ exposure for abemaciclib was 562 nM (Shapiro et al., 2013). Using similar calculations as with palbociclib, mean unbound brain concentrations in these patients are estimated to be 1.5 nM. Thus, the TER values for abemaciclib are 2.5 (CDK4) and 0.6 (CDK6), which is ~10-fold greater than the projected CDK4 TER of 0.2 for palbociclib, and supports an expectation that abemaciclib should potentially reach concentrations that inhibit the target enzymes in brain tumors. If the unbound brain concentrations are prolonged as observed in rat, then time-on-target might enhance the probability of clinical target engagement in the brain with abemaciclib. Admittedly, such calculations are not only subject to differences across species but also compounded variabilities inherent to the multiple assays used, e.g., in vitro IC_{50} or K_i, unbound fractions, and in vivo biosample levels, etc. The equilibrium dialysis method for measuring unbound fraction, especially using brain homogenate, is considered reliable for estimating free brain concentration within 3-fold, and rodent $f_{u,brain}$ is considered useful for predicting any species including human (Liu et al., 2009; Read and Braggio, 2010).

The preclinical data presented here show that abemaciclib crosses the BBB and confirm that both CDK4 and CDK6 inhibitors can reach unbound brain levels in rodents that would be expected to produce enzyme inhibition. However, abemaciclib brain levels are more efficiently reached at presumably lower doses than palbociclib and are possibly on target longer. Accordingly, abemaciclib alone had antitumor activity in the orthotopic glioblastoma U87MG xenograft rat model and showed apparent additive efficacy when co-dosed with TMZ.

ACKNOWLEDGMENTS

The authors thank Dr. Raquel Torres, PhD, Quantitative Biology-Spain for sharing unpublished data and Ms. Melissa Trowbridge, Covance Laboratories, Greenfield, IN for technical support. We also thank Anastasia Perkowski, Eli Lilly and Company, Bridgewater, NJ for helpful editorial comments and Dr. Richard Higgs for re-analyzing some of the efficacy data.

AUTHORSHIP CONTRIBUTIONS

Participated in research design: Raub, Gelbert, Wishart, Kulanthaivel, Shannon.

Conducted experiments: Staton, Ajamie, Sawada, Shannon.

Performed data analysis: Raub, Gelbert, Wishart, Kulanthaivel, Shannon, Sawada

Wrote or contributed to the writing of the manuscript: Raub, Gelbert, Sanchez-Martinez, De Dios.

REFERENCES

Agarwal S, Hartz AM, Elmquist WF, Bauer B (2011a) Breast cancer resistance protein and P-glycoprotein in brain cancer: two gatekeepers team up. Curr Pharm Des 17(26):2793-2802.

Agarwal S, Sane R, Oberoi R, Ohlfest JR, Elmquist WF (2011b) Delivery of molecularly targeted therapy to malignant glioma, a disease of the whole brain. Expert Rev Mol Med 13:e17.

Agarwal S, Manchanda P, Vogelbaum MA, Ohlfest JR, Elmquist WF (2013) Function of the blood-brain barrier and restriction of drug delivery to invasive glioma cells: findings in an orthotopic rat xenograft model of glioma. Drug Metab Dispos 41(1):33-39.

Blagosklonny MV, Pardee AB (2002) The restriction point of the cell cycle. Cell Cycle 1:103-110.

Cancer Genome Atlas Research Network (2008) Comprehensive genomic characterization defines human glioblastoma genes and core pathways. Nature 455:1061-1068.

Carcaboso AM, Elmeliegy MA, Shen J, Juel SJ, Zhang ZM, Calabrese C, Tracey L, Waters CM, Stewart CF (2010) Cancer Res 70: 4499–4508.

Chamberlain MC (2010) Anticancer therapies and CNS relapse: overcoming blood-brain and blood-cerebrospinal fluid barrier impermeability. Expert Rev Neurother 10(4):547–561.

Chu X, Bleasby K, Evers R. Species differences in drug transporters and implications for translating preclinical findings to humans (2013) Expert Opin Drug Metab Toxicol 9(3):237-252.

Cisternino S, Bourasset F, Archimbaud Y, Sémiond D, Sanderink G, Scherrmann JM (2003) Nonlinear accumulation in the brain of the new taxoid TXD258 following saturation of P-glycoprotein at the blood-brain barrier in mice and rats. British Journal of Pharmacology 138:1367–1375.

Dantzig AH, Shepard RL, Law KL, Tabas L, Pratt S, Gillespie JS, Binkley SN, Kuhfeld MT, Starling JJ, Wrighton SA (1999) Selectivity of the multidrug resistance modulator, LY335979, for P-glycoprotein and effect on cytochrome P450 activities. J Pharm Exper Ther 290: 854–890.

Desai PV, Sawada GA, Watson IA, Raub TJ (2013) Integration of in silico and in vitro tools for scaffold optimization during drug discovery: predicting P-glycoprotein efflux. Mol Pharm 10(4):1249-1261.

de Vries NA, Beijnen JH, van Tellingen O (2009) High-grade glioma mouse models and their applicability for preclinical testing. Cancer Treatment Reviews 35:714–723.

Deeken JF, Loscher W (2007) The blood-brain barrier and cancer: transporters, treatment, and Trojan horses. Clinical Cancer Research: an official journal of the American Association for Cancer Research 13:1663-1674.

Dempsey JA, Chan EM, Burke TF, Beckmann RP (2013) LY2835219, a selective inhibitor of CDK4 and CDK6, inhibits growth in preclinical models of human cancer. http://www.abstractsonline.com/Plan/ViewAbstract.aspx?mID=3086&sKey=8786ea1b-3082-4160-87ee-e7cfa17623d0&cKey=74a48bbf-b1b4-4f91-b152-af8cbb488509&mKey=9b2d28e7-24a0-466f-a3c9-07c21f6e9bc9 AACR Meeting Abstract LB-122.

Di L, Rong H, Feng B (2013) Demystifying brain penetration in central nervous system drug discovery. Miniperspective. J Med Chem 56:2-12.

Dyson N (1998) The regulation of E2F by pRB-family proteins. Genes & development 12:2245-2262.

Eichler AF, Loeffler JS (2007) Multidisciplinary management of brain metastases. The Oncologist 12:884-898.

Fattori S, Becherini F, Cianfriglia M, Parenti G, Romanini A, Castagna M (2007) Human brain tumors: multidrug-resistance P-glycoprotein expression in tumor cells and intratumoral capillary endothelial cells. Virchows Arch 451:81–87.

Flaherty KT, Fisher DE (2011) New strategies in metastatic melanoma: oncogene-defined taxonomy leads to therapeutic advances. Clin Cancer Res 17:4922-4928.

Flaherty KT, Lorusso PM, Demichele A, Abramson VG, Courtney R, Randolph SS, Shaik MN, Wilner KD, O'Dwyer PJ, Schwartz GK (2012) Phase I, dose-escalation trial of the oral cyclin-dependent kinase 4/6 inhibitor PD 0332991, administered using a 21-day schedule in patients with advanced cancer. Clin Cancer Res 18:568-576.

Fortin D (2012) The blood-brain barrier: its influence in the treatment of brain tumors metastases. Curr Cancer Drug Targets 12:247-259.

Friedman HS, Kerby T, Calvert H (2000) Temozolomide and treatment of malignant glioma. Clin Cancer Res 6:2585-2597.

Gelbert LM, Cai S, Lin X, Sanchez-Martinez C, del Prado M, Lallena MJ, Torres R, Ajamie RT, Wishart GN, Flack RS, Neubauer BL, Young J, Chan EM, Iversen P, Cronier D, Kreklau E, de Dios A (2014) Preclinical characterization of the CDK4/6 inhibitor LY2835219: in-vivo cell cycle-dependent/independent anti-tumor activities alone/in combination with gemcitabine. Invest New Drugs 32(5):825-837.

Geldof M, Freijer J, van Beijsterveldt L, Danhof M (2008) Pharmacokinetic modeling of non-linear brain distribution of fluvoxamine in the rat. Pharm Res 25:792-804.

Gerstner ER, Fine RL (2007) Increased permeability of the blood-brain barrier to chemotherapy in metastatic brain tumors: establishing a treatment paradigm. J Clin Oncol 25(16):2306-2312.

Hammarlund-Udenaes M, Fridén M, Syvänen S, Gupta A (2008) On the rate and extent of drug delivery to the brain. Pharm Res 25:1737-1750.

Jacobs VL, Valdes PA, Hickey WF, De Leo JA (2011) Current review of in vivo GBM rodent models: emphasis on the CNS-1 tumour model. ASN Neuro 3:e00063.

Jiang Z, Pore N, Cerniglia GJ, Mick R, Georgescu MM, Bernhard EJ, Hahn SM, Gupta AK, Maity A (2007) Phosphatase and tensin homologue deficiency in glioblastoma confers resistance to radiation and temozolomide that is reversed by the protease inhibitor nelfinavir. Cancer Res 67(9):4467-4473.

Kalvass JC, Maurer TS (2002) Influence of nonspecific brain and plasma binding on CNS exposure: Implications for rational drug discovery. Biopharm Drug Dispos 23:327–338.

Kalvass JC, Polli JW, Bourdet DL, Feng B, Huang SM, Liu X, Smith QR, Zhang LK, Zamek-Gliszczynski MJ; International Transporter Consortium (2013) Why clinical modulation of efflux

transport at the human blood-brain barrier is unlikely: the ITC evidence-based position. Clin Pharmacol Ther 94:80-94.

Kodaira H, Kusuhara H, Ushiki J, Fuse E, Sugiyama Y (2010) Kinetic analysis of the cooperation of P-glycoprotein (P-gp/Abcb1) and breast cancer resistance protein (Bcrp/Abcg2) in limiting the brain and testis penetration of erlotinib, flavopiridol, and mitoxantrone. J Pharmacol Exp Ther 333(3):788-796.

Landis MW, Pawlyk BS, Li T, Sicinski P, Hinds PW (2006) Cyclin D1-dependent kinase activity in murine development and mammary tumorigenesis. Cancer Cell 9:13-22.

Langer CJ, Mehta MP (2005) Current management of brain metastases, with a focus on systemic options. J Clin Oncol 23:6207-6219.

Lee J, Lund-Smith C, Borboa A, Gonzalez AM, Baird A, Eliceiri BP (2009) Glioma-induced remodeling of the neurovascular unit. Brain Res 1288:125-134.

Lin NU, Carey LA, Liu MC, Younger J, Come SE, Ewend M, Harris GJ, Bullitt E, Van den Abbeele AD, Henson JW, Li X, Gelman R, Burstein HJ, Kasparian E, Kirsch DG, Crawford A, Hochberg F, Winer EP (2008) Phase II trial of lapatinib for brain metastases in patients with human epidermal growth factor receptor 2-positive breast cancer. J Clin Oncol 26:1993-1999.

Liu X, Van Natta K, Yeo H, Vilenski O, Weller PE, Worboys PD, Monshouwer M (2009) Unbound drug concentration in brain homogenate and cerebral spinal fluid at steady state as a surrogate for unbound concentration in brain interstitial fluid. Drug Metab Dispos 37:787-793.

Lockman PR, Mittapalli RK, Taskar KS, Rudraraju V, Gril B, Bohn KA, Adkins CE, Roberts A, Thorsheim HR, Gaasch JA, Huang S, Palmieri D, Steeg PS, Smith QR (2010) Heterogeneous blood-tumor barrier permeability determines drug efficacy in experimental brain metastases of breast cancer. Clin Cancer Res 16:5664-5678.

Lundberg AS, Weinberg RA (1998) Functional inactivation of the retinoblastoma protein requires sequential modification by at least two distinct cyclin-cdk complexes. Mol Cell Biol 18:753-761.

Malumbres M, Barbacid M (2001) To cycle or not to cycle: a critical decision in cancer. Nat Rev Cancer 1:222-231.

Malumbres M, Barbacid M (2006) Is Cyclin D1-CDK4 kinase a bona fide cancer target? Cancer Cell 9:2-4.

Michaud K, Solomon DA, Oermann E, Kim JS, Zhong WZ, Prados MD, Ozawa T, James CD, Waldman T (2010) Pharmacologic inhibition of cyclin-dependent kinases 4 and 6 arrests the growth of glioblastoma multiforme intracranial xenografts. Cancer Res 70:3228-3238.

Motl S, Zhuang Y, Waters CM, Stewart CF (2006) Pharmacokinetic considerations in the treatment of CNS tumours. Clin Pharmacokinet 45:871-903.

Ohgaki H, Kleihues P. Epidemiology and etiology of gliomas (2005) Acta Neuropathologica 109:93-108.

Ortega S, Malumbres M, Barbacid M (2002) Cyclin D-dependent kinases, INK4 inhibitors and cancer. Biochimica et Biophysica Acta 1602:73-87.

Padowski JM, Pollack GM (2011) Influence of time to achieve substrate distribution equilibrium between brain tissue and blood on quantitation of the blood-brain barrier P-glycoprotein effect. Brain Res 1426:1-17.

Pardee AB (1974) A restriction point for control of normal animal cell proliferation. Proc Natl Acad Sci USA 71:1286-1290.

Parsons DW, Jones S, Zhang X, Lin JC, Leary RJ, Angenendt P, Mankoo P, Carter H, Siu IM, Gallia GL, Olivi A, McLendon R, Rasheed BA, Keir S, Nikolskaya T, Nikolsky Y, Busam DA, Tekleab H, Diaz LA Jr, Hartigan J, Smith DR, Strausberg RL, Marie SK, Shinjo SM, Yan H, Riggins GJ, Bigner DD, Karchin R, Papadopoulos N, Parmigiani G, Vogelstein B, Velculescu VE, Kinzler KW (2008) An integrated genomic analysis of human glioblastoma multiforme. Science 321:1807-1812.

Patchell RA (2003) The management of brain metastases. Cancer Treat Rev 29:533.

Polli JW, Olson KL, Chism JP, John-Williams LS, Yeager RL, Woodard SM, Otto V, Castellino S, Demby VE (2009) An unexpected synergist role of P-glycoprotein and breast cancer resistance protein on the central nervous system penetration of the tyrosine kinase inhibitor lapatinib (N-{3-chloro-4-[(3-fluorobenzyl)oxy]phenyl}-6-[5-({[2-(methylsulfonyl)ethyl]amino}methyl)-2-furyl]-4-quinazolinamine; GW572016). Drug Metab Dispos 37:439-442.

Radaelli E, Ceruti R, Patton V, Russo M, Degrassi A, Croci V, Caprera F, Stortini G, Scanziani E, Pesenti E, Alzani R (2009) Immunohistopathological and neuroimaging characterization of murine orthotopic xenograft models of glioblastoma multiforme recapitulating the most salient features of human disease. Histol Histopathol 24:879-891.

Raub TJ, Lutzke BS, Andrus PK, Sawada GA, Staton BA (2006) Early preclinical evaluation of brain exposure in support of hit identification and lead optimization. In Optimizing the ”Drug-Like” Properties of Leads in Drug Discovery, Biotechnology: Pharmaceutical Aspects Series, R.T. Borchardt, C.R. Middaugh, eds; Springer, pp. 355-410.

Read KD, Braggio S (2010) Assessing brain free fraction in early drug discovery. Expert Opin Drug Metab Toxicol 6:337-644.

Reifenberger G, Reifenberger J, Ichimura K, Collins VP (1995) Amplification at 12q13-14 in human malignant gliomas is frequently accompanied by loss of heterozygosity at loci proximal and distal to the amplification site. Cancer Res 55:731-734.

Robey RW, Honjo Y, Morisaki K, Nadjem TA, Runge S, Risbood M, Poruchynsky MS, Bates SE (2003) Mutations at amino-acid 482 in the ABCG2 gene affect substrate and antagonist specificity. Br J Cancer 89:1971-1978.

Salphati L, Heffron TP, Alicke B, Nishimura M, Barck K, Carano RA, Cheong J, Edgar KA, Greve J, Kharbanda S, Koeppen H, Lau S, Lee LB, Pang J, Plise EG, Pokorny JL, Reslan HB, Sarkaria JN, Wallin JJ, Zhang X, Gould SE, Olivero AG, Phillips HS (2012) Targeting the PI3K pathway in the brain--efficacy of a PI3K inhibitor optimized to cross the blood-brain barrier. Clin Cancer Res 18:6239-6248.

Sane R, Agarwal S, Elmquist WF (2012) Brain distribution and bioavailability of elacridar after different routes of administration in the mouse. Drug Metab Dispos 40:1612-1619.

Schmidt EE, Ichimura K, Reifenberger G, Collins VP (1994) CDKN2 (p16/MTS1) gene deletion or CDK4 amplification occurs in the majority of glioblastomas. Cancer Res 54:6321-6324.

Shapiro G, Rosen LS, Tolcher AW, Goldman JW, Gandhi L, Papadopoulos KP, et al (2013) A first-in-human phase I study of the CDK4/6 inhibitor, LY2835219, for patients with advanced cancer. J Clin Oncol 31, (suppl; abstr 2500) http://meetinglibrary.asco.org/content/111069-132.

Sharom FJ (2008) ABC multidrug transporters: structure, function and role in chemoresistance. Pharmacogenomics 9:105-127.

Siena S, Crino L, Danova M, Del Prete S, Cascinu S, Salvagni S, Schiavetto I, Vitali M, Bajetta E (2010) Dose-dense temozolomide regimen for the treatment of brain metastases from melanoma, breast cancer, or lung cancer not amenable to surgery or radiosurgery: a multicenter phase II study. Ann Oncol 21:655-661.

Steeg PS, Camphausen KA, Smith QR (2011) Brain metastases as preventive and therapeutic targets. Nat Rev Cancer 11:352-363.

Taskar KS, Rudraraju V, Mittapalli RK, Samala R, Thorsheim HR, Lockman J, Gril B, Hua E, Palmieri D, Polli JW, Castellino S, Rubin SD, Lockman PR, Steeg PS, Smith QR (2012) Lapatinib distribution in HER2 overexpressing experimental brain metastases of breast cancer. Pharm Res 29:770–781.

Tombline G, Holt JJ, Gannon MK, Donnelly DJ, Wetzel B, Sawada GA, Raub TJ, Detty MR (2008) ATP occlusion by P-glycoprotein as a surrogate measure for drug coupling. Biochem 47:3294-307.

Vogelbaum M, Thomas T (2007) Small molecular agents. In: Barnett GH, ed. High-Grade Gliomas: Diagnosis and Treatment. Totowa, NJ: Humana Press; 337-356.

Wager TT, Villalobos A, Verhoest PR, Hou X, Shaffer CL (2011) Strategies to optimize the brain availability of central nervous system drug candidates. Expert Opin Drug Discov 6:371-381.

Yu Q, Sicinska E, Geng Y, Ahnstrom M, Zagozdzon A, Kong Y, Gardner H, Kiyokawa H, Harris LN, Stål O, Sicinski P. (2006) Requirement for CDK4 kinase function in breast cancer. Cancer Cell 9:23-32.

Zamek-Gliszczynski MJ, Sprague KE, Espada A, Raub TJ, Morton SM, Manro JR, Molina-Martin M (2012) How well do lipophilicity parameters, MEEKC microemulsion capacity factor, and plasma protein binding predict CNS tissue binding? J Pharm Sci 101:1932-1940.

Zhang S, Yang X, Morris ME (2004) Flavonoids are inhibitors of breast cancer resistance protein (ABCG2)-mediated transport. Mol Pharmacol 65:1208-1216.

FOOTNOTES

Disclosure of Potential Conflicts of Interest: All Lilly authors are or were Eli Lilly and Company employees and shareholders. Lawrence M. Gelbert and Harlan E. Shannon are now Adjunct Professors, Pediatrics Hematology/Oncology in the HB Wells Center for Pediatric Research at Indiana University. Brian A. Staton is currently employed by Quintiles Company. The authors disclose no potential conflicts of interest.

Lawrence M. Gelbert and Harlan E. Shannon current address: Department of Pediatrics, Herman B. Wells Center for Pediatric Research, Division of Hematology/Oncology, Simon Cancer Center, Indiana University School of Medicine, Indianapolis, IN 46202

Brian A. Staton current address: Advion Bioanalytical Laboratories, A Quintiles Company, Indianapolis, IN 46241

DMD Fast Forward. Published on July 6, 2015 as DOI: 10.1124/dmd.114.062745
This article has not been copyedited and formatted. The final version may differ from this version.

FIGURES

Figure 1. Unbound plasma and brain exposures for abemaciclib dosed orally once in normal CD-1 mice at 30 mg/kg and samples analyzed at intervals over 24 hours. Total exposures were corrected for protein binding using the measured unbound fraction (Table 4). The data are mean and standard deviation of triplicate animals. The reference concentrations are 1) P-gp EC_{50} of 95 nM or the mean unbound plasma concentration where 50% of the BBB P-gp is saturated as determined in Fig. 2, 2) CDK4/cyclinD1 K_i^{ATP} of 0.6 nM or the mean unbound concentration where 50% of the enzyme is inhibited in vitro (Gelbert et al., 2014), and 3) and CDK6/cyclinD1 K_i^{ATP} of 2.4 nM or the mean unbound concentration where 50% of the enzyme is inhibited in vitro (Gelbert et al., 2014).

Figure 2. Exposure-dependent increase in brain-to-plasma ratios (Kp) relative to total and unbound plasma exposure for abemaciclib and palbociclib. Wild-type CF-1 mice were dosed intravenously (bolus) at 0.5, 2.2, 5.4, and 10.9 µmole/kg and plasma and brain levels measured at 5-min. Kp is plotted against total and unbound (fu,abemaciclib = 0.054; fu,palbociclib = 0.23) plasma concentrations. Values are mean and standard deviation of triplicate animals and are reported in Supplement Table 1.

Figure 3. Unbound plasma and brain exposures for abemaciclib and palbociclib dosed orally once in rats at 30 mg/kg and samples analyzed at intervals over 48 hours. Total exposures were corrected for protein binding using the measured fraction unbound (Table 4). The data are mean and standard deviation of triplicate animals. The reference concentrations for abemaciclib are 1) CDK4/cyclinD1 K_i^{ATP} of 0.6 nM, or the mean unbound concentration where 50% of the enzyme is inhibited in vitro (Gelbert et al., 2014), and 2) CDK6/cyclinD1 K_i^{ATP} of 2.4 nM, or the mean unbound concentration where 50% of the enzyme is inhibited in vitro (Gelbert et al., 2014).

Figure 4. Distribution of abemaciclib-related radioactivity in brain tissues. SD rats were administered a single 10-mg/kg oral dose of [^{14}C] abemaciclib and the tissue concentrations were determined by quantitative whole-body autoradiography (Supplemental Figure 1). Data are presented as tissue-to-plasma AUC (A) and Cmax (B) ratios.

Figure 5. Dose-dependent anti-tumor activity of abemaciclib in an orthotopic U87MG rat glioma model. Tumor-bearing animals were treated for 21 days with abemaciclib beginning on day 4 (bold bar). A) Anti-tumor effect of abemaciclib as indicated by increased survival of animals. Median survival was increased by 3, 7.5 and 10 days for the 20 mg/kg, 40 mg/kg and 80 mg/kg doses, respectively (Table). B) Total and unbound plasma and brain exposures of abemaciclib were determined in non-tumor bearing rats after four-daily doses and 24 h after last dose. Animals (N=2) were euthanized 24 hours after last dose. Total exposures were corrected for protein binding using the measured fraction unbound (Table 4). The reference concentrations are 1) P-gp EC_{50} of 95 nM or the mean unbound plasma concentration where 50% of the BBB P-gp is saturated as determined in Fig. 2, 2) CDK4/cyclinD1 K_i^{ATP} of 0.6 nM or the mean unbound concentration where 50% of the enzyme is inhibited in vitro (Gelbert et al., 2014), and 3) and CDK6/cyclinD1 K_i^{ATP} of 2.4 nM or the mean unbound concentration where 50% of the enzyme is inhibited in vitro (Gelbert et al., 2014).

Figure 6. In vivo antitumor activity of abemaciclib in combination with temozolomide. Subcutaneous U87MG glioblastoma xenografts were treated with abemaciclib by oral gavage daily for 21 days, with temozolomide by intraperitoneal injection every 7 days for a total of 2 doses, or both compounds together. Treatment period is indicated by the horizontal black line next to the x-axis, and the effect on body weight shown in the upper left corner.

Figure 7. Combinations of abemaciclib and temozolomide are additive in a rat orthotopic glioma model. Treatments were started on day 6 at the indicated dose and schedule (horizontal bar next to X axis indicates treatment period). All treatments resulted in a statistically significant increase in survival, with the combination of abemaciclib daily/TMZ resulting in an additive effect, and the combination of abemaciclib every other day/TMZ resulting in a greater than additive effect (Table).

DMD Fast Forward. Published on July 6, 2015 as DOI: 10.1124/dmd.114.062745
This article has not been copyedited and formatted. The final version may differ from this version.

TABLES

Table 1. Physicochemical properties of abemaciclib and palbociclib

Property	**abemaciclib**	**palbociclib**
Chemical Structure	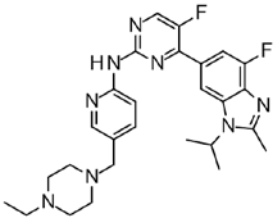	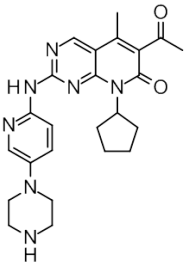
Molecular weight, daltons	507	448
clogP[1]	4.3 (3.36*)	2.8 (2.29)
cpK_a[1]	8.4 (7.9)	8.9 (8.4)
logD[2] pH 6	(1.39)	(-0.12)
clogD[1] pH 7.4	3.4 (2.70)	1.3 (1.25)
Polar surface area[1], Å[2]	75	105
H-bond donor number	1	2
H-bond acceptor number	8	9
Aqueous solubility[3], mg/mL	>2 at pH 4.5; 0.012 at pH 7.5	>2 at pH 2.0; 0.033 at pH 7.6

[1] Calculated log octanol-water partition coefficient (clogP), calculated negative logarithm of the acid dissociation constant (cpK_a), and calculated log octanol-water partition coefficient at a specific pH (clogD) were obtained using Chemaxon. Polar surface area (PSA) was obtained from a Novartis version of a prediction algorithm that estimates the sum of the molecular surface area contributed by N, O atoms and/or H atom bonded with N or O in a molecule.

[2] logP and logD were measured using an automated potentiometric method (Sirius Analytical, East Sussex, UK).

[3] Solubility was measured at equilibrium in phosphate buffer.

*All values in parentheses are measured.

DMD Fast Forward. Published on July 6, 2015 as DOI: 10.1124/dmd.114.062745
This article has not been copyedited and formatted. The final version may differ from this version.

Table 2. Bidirectional flux studies using MDCK cell monolayers that overexpress human P-glycoprotein. Inhibition with 2.5 µM LSN335984. Average values from duplicate test runs where variability is <22%.

Compound	**Inhibitor**	**A-B P_{app}, nm/sec**	**B-A P_{app}, nm/sec**	**%Cell**[1]	**Efflux Ratio**[2]	**Net Efflux Ratio**[2]	**Calcein-AM % Inhibition**[3]
abemaciclib	-	12	49	68	4.1	5.1	30, 64
	+	19	16	56	0.8		
palbociclib	-	60	720	46	12	8.6	1, 3
	+	150	210	32	1.4		

[1] Estimated buffer/cell distribution coefficient defined as the fraction of mass that was added to the donor and recovered in the methanol rinse.
[2] Efflux Ratio (ER) is basolateral (B)-apical (A) P_{app}/A-B P_{app}. Net Efflux Ratio is ER without inhibitor/ER with inhibitor.
[3] Inhibition of Calcein-AM uptake into MDCK-P-gp cells at 5 and 25 µM relative to inhibition using 5 µM LSN335984.

DMD Fast Forward. Published on July 6, 2015 as DOI: 10.1124/dmd.114.062745
This article has not been copyedited and formatted. The final version may differ from this version.

Table 3. Bidirectional flux studies using MDCK cell monolayers that overexpress mouse bcrp. Inhibition with 20 μM chrysin. Average values from duplicate test runs where variability is <18%.

Compound	**Inhibitor**	**A-B P_{app}, nm/sec**	**B-A P_{app}, nm/sec**	**%Cell**[1]	**Efflux Ratio**[2]	**Net Efflux Ratio**[2]	**Bodipy-prazosin % Inhibition**[3]
abemaciclib	-	38	410	58	11	9	29, 47
	+	94	110	52	1.2		
palbociclib	-	72	1180	4.4	16	11	21, 39
	+	310	480	24	1.5		

[1] Estimated buffer/cell distribution coefficient defined as the fraction of mass that was added to the donor and recovered in the methanol rinse.
[2] Efflux Ratio (ER) is basolateral (B)-apical (A)P_{app}/A-B P_{app}. Net Efflux Ratio is ER without inhibitor/ER with inhibitor.
[3] Inhibition of Bodipy-prazosin uptake into MDCK-bcrp cells at 5 and 25 μM relative to inhibition using 20 μM chrysin.

DMD Fast Forward. Published on July 6, 2015 as DOI: 10.1124/dmd.114.062745
This article has not been copyedited and formatted. The final version may differ from this version.

Table 4. Percentage of unbound fraction in plasma and brain homogenate for three species.

Compound	**Plasma**[1]			**Brain**[2]		
	Mouse	**Rat**	**Human**	**Mouse**	**Rat**	**Human**
abemaciclib	5.4 ± 0.4	3.7 ± 0.3	2.7 ± 0.3	0.79 ± 0.03	0.43 ± 0.05	ND
palbociclib	23 ± 1	21 ± 3	ND	2.0 ± 0.1	2.7 ± 0.2	ND

[1] Stock solutions of test compounds were added to plasma to give final concentrations of 0.1% DMSO and 1 µM compound.

[2] Brain homogenate was prepared in 100 mM phosphate buffer (1:3, w/v; pH 7.4) by probe sonication.

ND, not determined.

DMD Fast Forward. Published on July 6, 2015 as DOI: 10.1124/dmd.114.062745
This article has not been copyedited and formatted. The final version may differ from this version.

Table 5. Mouse and rat PK for abemaciclib using a 30-mg/kg oral dose. Data are mean values from three animals.

Parameter	**Mouse**	**Rat**	**Units**
Plasma $AUC_{0\text{-}24\ h}$	69,300	52,300	ng·h/mL
Plasma $AUC_{0\text{-}24\ h}$	136,686	103,156	nM·h
Unbound[1] Plasma $AUC_{0\text{-}24\ h}$	7,381	3,817	nM·h
Plasma T_{max}[2]	4	3.3	h
Plasma C_{max}	8,470	1,500	ng/mL
Plasma C_{max}	16,706	2,958	nM
Unbound[1] Plasma C_{max}	902	109	nM
Brain $AUC_{0\text{-}24\ h}$	13,200	47,900	ng·h/mL
Brain $AUC_{0\text{-}24\ h}$	26,035	94,447	nM·h
Unbound Brain $AUC_{0\text{-}24\ h}$	206	406	nM·h
Brain T_{max}	2	4	h
Brain C_{max}	1,840	1,500	ng/mL
Brain C_{max}	3,629	2,958	nM
Unbound[1] Brain C_{max}	29	13	nM
Clearance[2]	41	14	mL/min/kg
Half life[2]	13	6	h
$V_{d,ss}$[2]	34	6.0	L/kg
Oral Bioavailability[2]	62	43	%

[1] Measured f_u values from Table 3.
[2] Determined from 1 mg/kg (mouse) or 0.5 mg/kg (rat) IV and 3 mg/kg (mouse) or 1.0 mg/kg (rat) PO doses.

DMD Fast Forward. Published on July 6, 2015 as DOI: 10.1124/dmd.114.062745
This article has not been copyedited and formatted. The final version may differ from this version.

Table 6. Mouse Brain Uptake Assay results for abemaciclib and palbociclib in CF-1 (normal) or CF-1 mdr1a(-/-) mice. Total concentrations in plasma and brain were measured five minutes after intravenous dose of 2.2 µmole/kg, brain concentrations were corrected for plasma volume and unbound concentrations calculated using the measured unbound fraction (Table 4).

Compounds	**$C_{u,plasma}$ (nM)**		**$C_{u,brain}$ (nM)**		**$K_{p,brain}$[1]**		**$K_{p,uu,brain}$[1]**	
	Normal	**KO**	**Normal**	**KO**	**Normal**	**KO**	**Normal**	**KO**
abemaciclib	120	141	20	67	1.2	3.2	0.17	0.48
palbociclib	478	344	6	71	0.1	2.3	0.01	0.21

[1] $K_{p,brain}$ is the brain-to-plasma ratio of the total concentrations. $K_{p,uu,brain}$ is the brain-to-plasma ratio of the unbound concentrations.

DMD Fast Forward. Published on July 6, 2015 as DOI: 10.1124/dmd.114.062745
This article has not been copyedited and formatted. The final version may differ from this version.

Table 7. Rat Brain Uptake Assay results for abemaciclib and palbociclib in Sprague-Dawley rats. Rats were dosed intravenously with vehicle (control) or vehicle containing 30 mg/kg of the P-gp inhibitor LSN335984 (+ Inhibitor) at 1 h before dosing with test compound at 2.2 µmole/kg. Total concentrations in plasma and brain were measured five minutes after intravenous dose, brain concentrations were corrected for plasma volume and unbound concentrations calculated using the measured unbound fraction (Table 4).

Compounds	**$C_{u,plasma}$ (nM)**		**$C_{u,brain}$ (nM)**		**$K_{p,brain}$[1]**		**$K_{p,uu,brain}$[1]**	
	Control	**+ Inhib**	**Control**	**+ Inhib**	**Control**	**+ Inhib**	**Control**	**+ Inhib**
abemaciclib	92	88	10	39	1.3	3.9	0.11	0.44
palbociclib	327	464	4	32	0.1	2.3	0.01	0.07

[1] $K_{p,brain}$ is the brain-to-plasma ratio of the total concentrations. $K_{p,uu,brain}$ is the brain-to-plasma ratio of the unbound concentrations.

Figure 1.

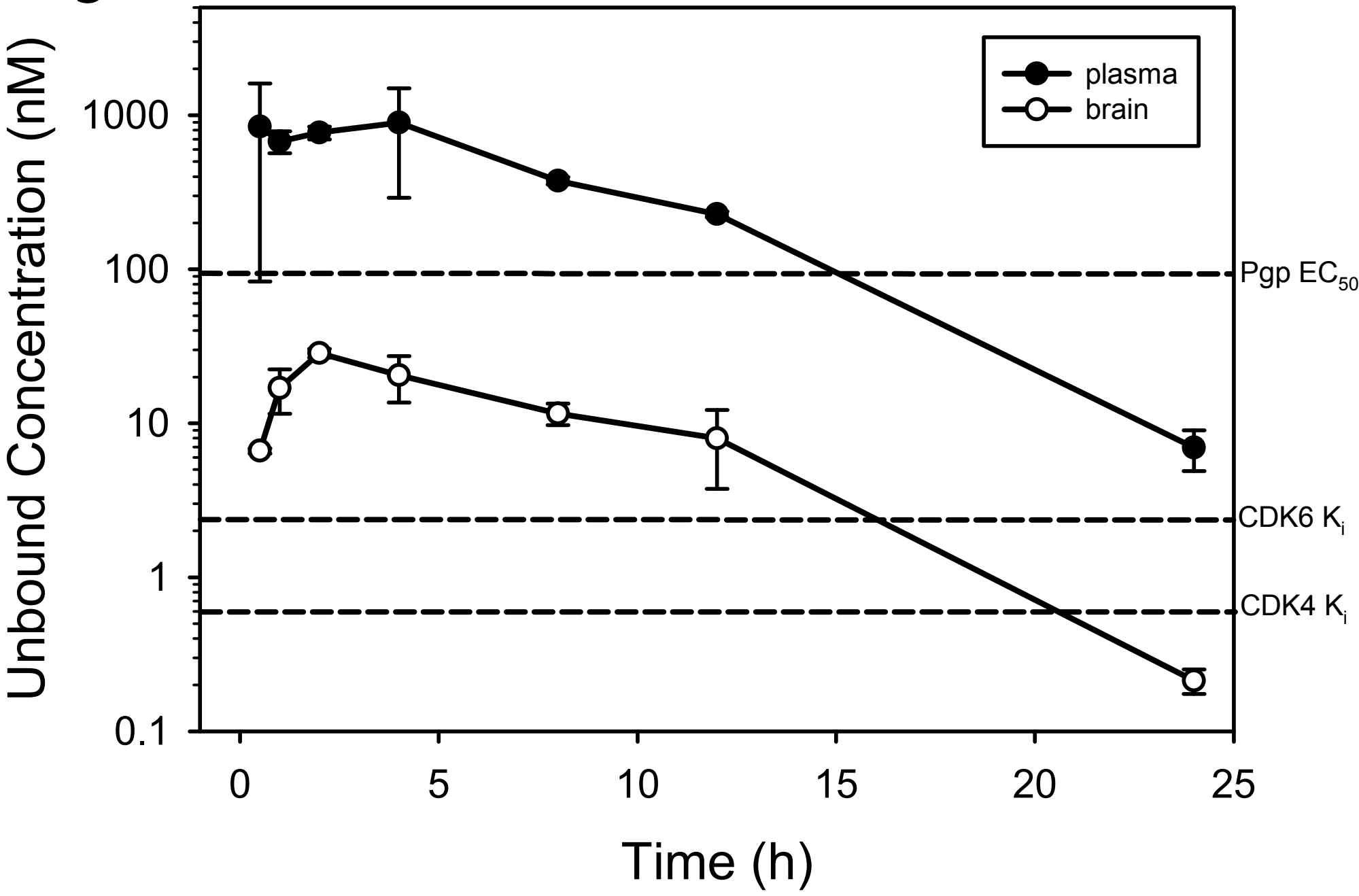
plasma
brain
Unbound Concentration (nM)
1000
100
10
1
0.1
Pgp EC50
CDK6 Ki
CDK4 Ki
0
5
10
15
20
25
Time (h)

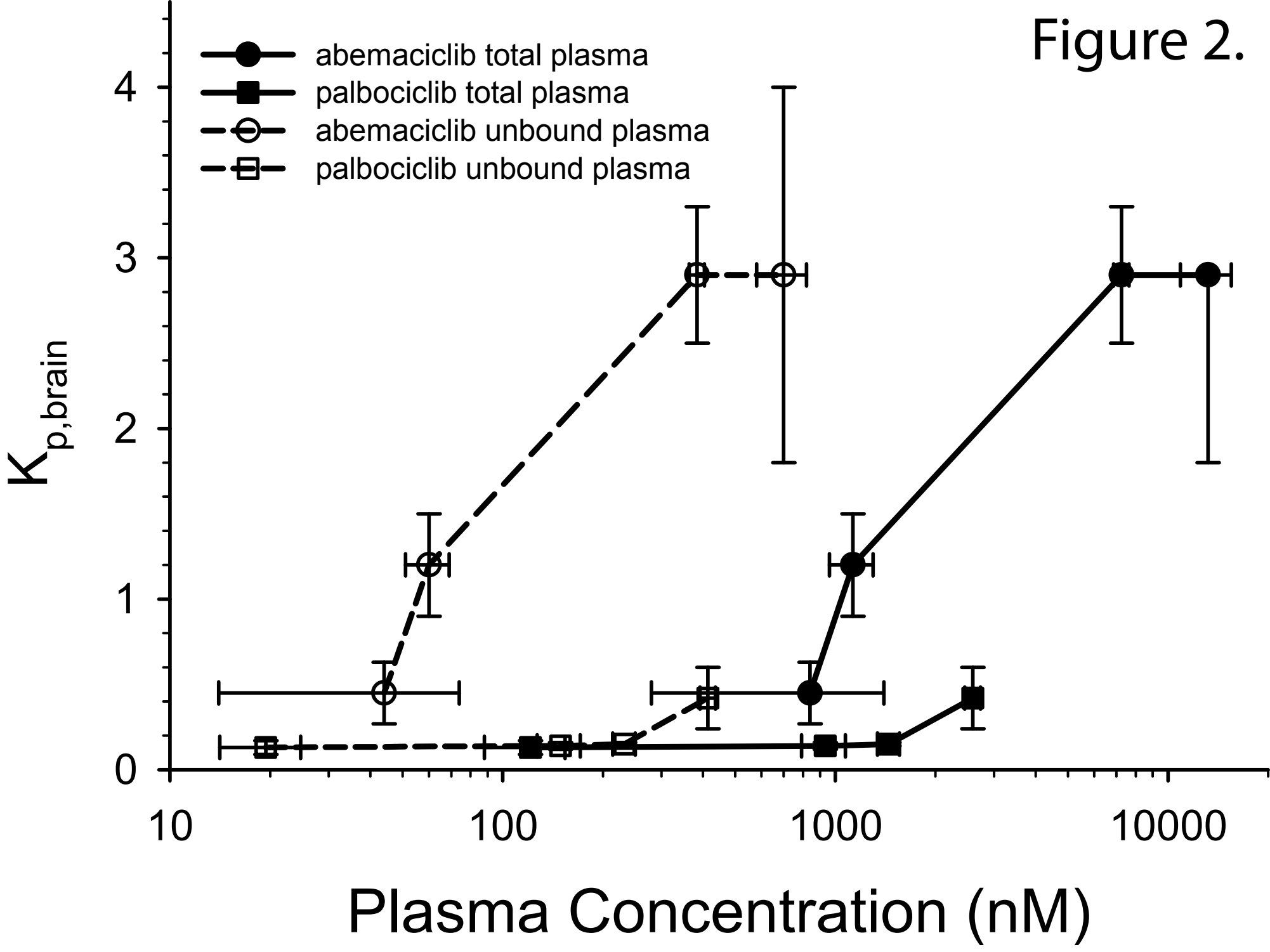
Figure 2.
abemaciclib total plasma
palbociclib total plasma
abemaciclib unbound plasma
palbociclib unbound plasma
$K_{p,brain}$
0
1
2
3
4
10
100
1000
10000
Plasma Concentration (nM)

Figure 3.

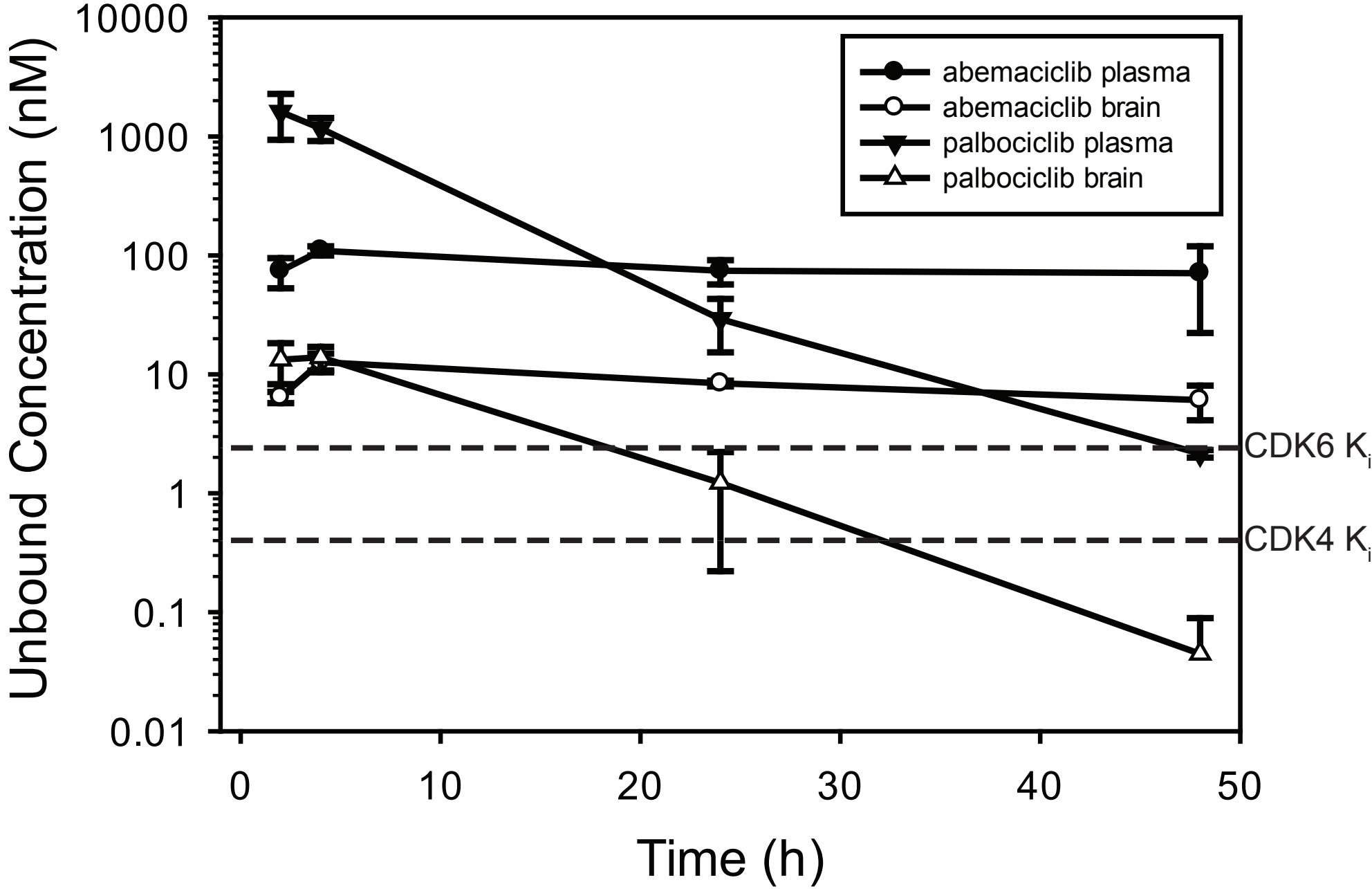
10000
1000
100
10
1
0.1
0.01
Unbound Concentration (nM)
0
10
20
30
40
50
Time (h)
abemaciclib plasma
abemaciclib brain
palbociclib plasma
palbociclib brain
CDK6 K$_i$
CDK4 K$_i$

Figure 4.

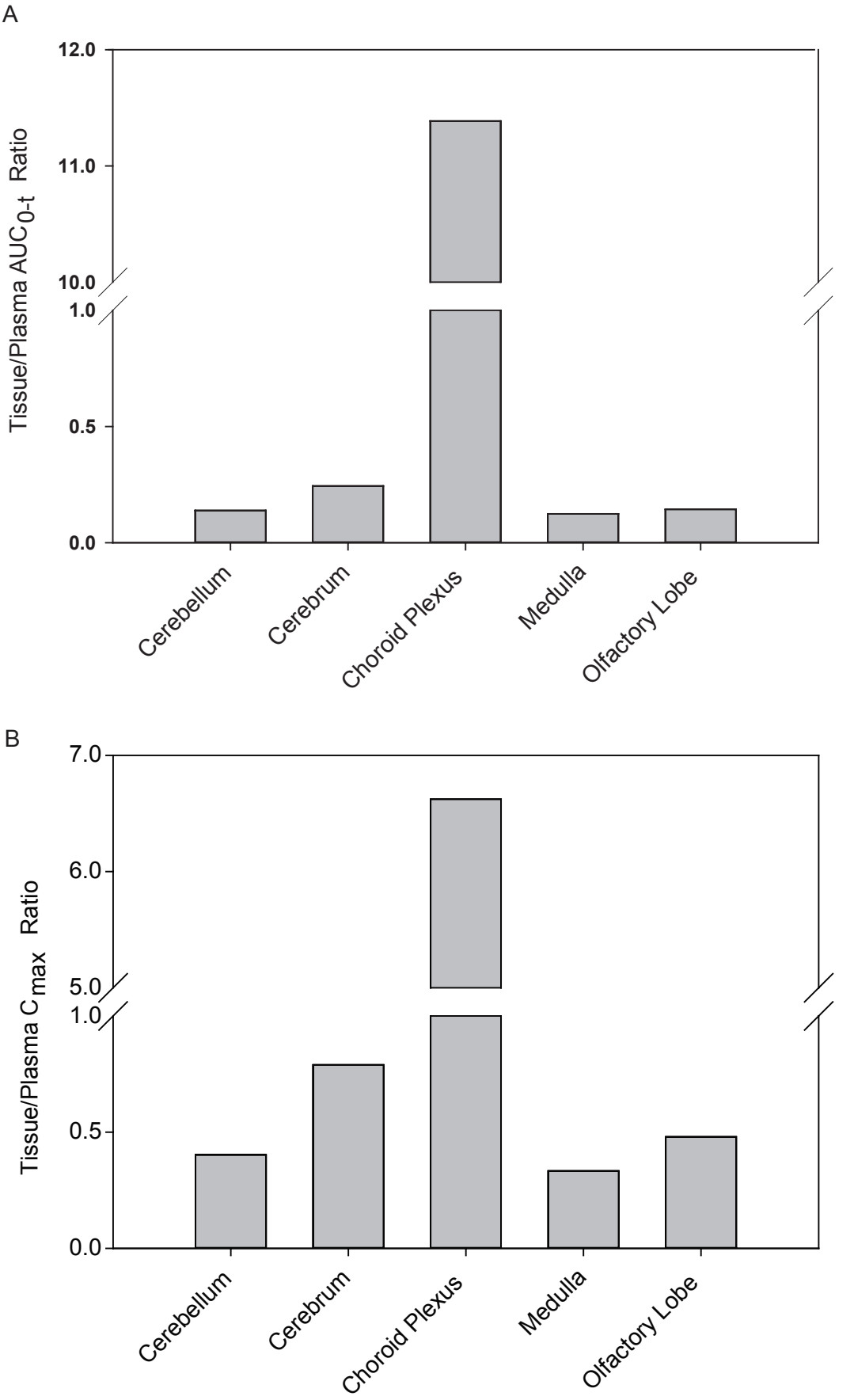
A
12.0
11.0
10.0
1.0
0.5
0.0
Tissue/Plasma AUC0-t Ratio
Cerebellum
Cerebrum
Choroid Plexus
Medulla
Olfactory Lobe
B
7.0
6.0
5.0
1.0
0.5
0.0
Tissue/Plasma Cmax Ratio
Cerebellum
Cerebrum
Choroid Plexus
Medulla
Olfactory Lobe

Figure 5.

A

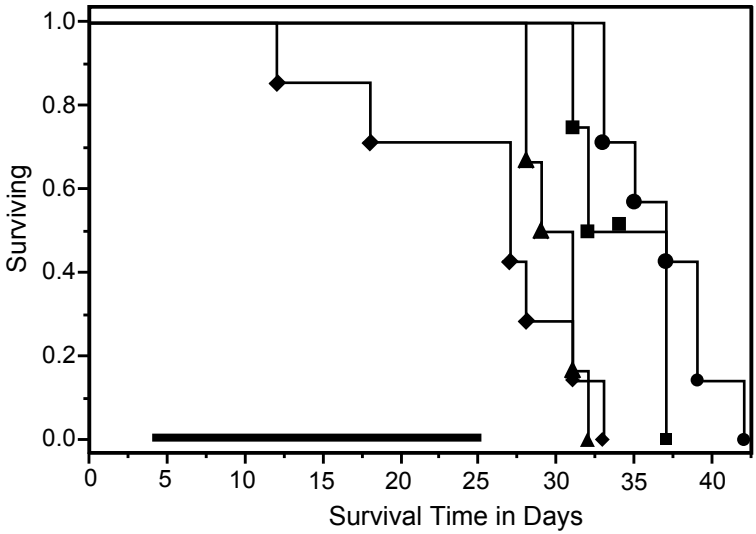

Symbol	Group (mg/kg)	N	Median (days)	p Value	Increase in Survival vs. Vehicle (days)
◆	Vehicle (0)	7	27	—	—
▲	Abemaciclib (20)	7	30	0.50	3
■	Abemaciclib (40)	6	34.5	0.032	7.5
●	Abemaciclib (80)	7	37	0.0006	10

B

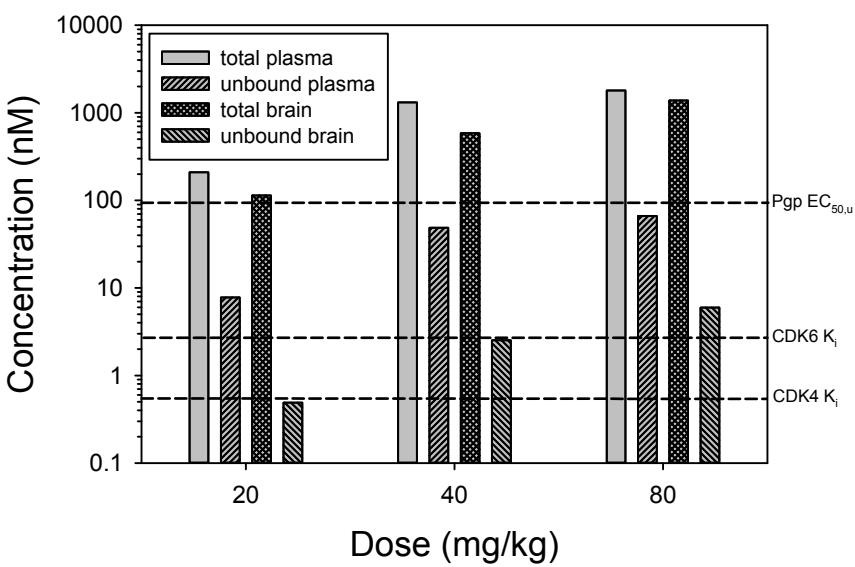

Figure 6.

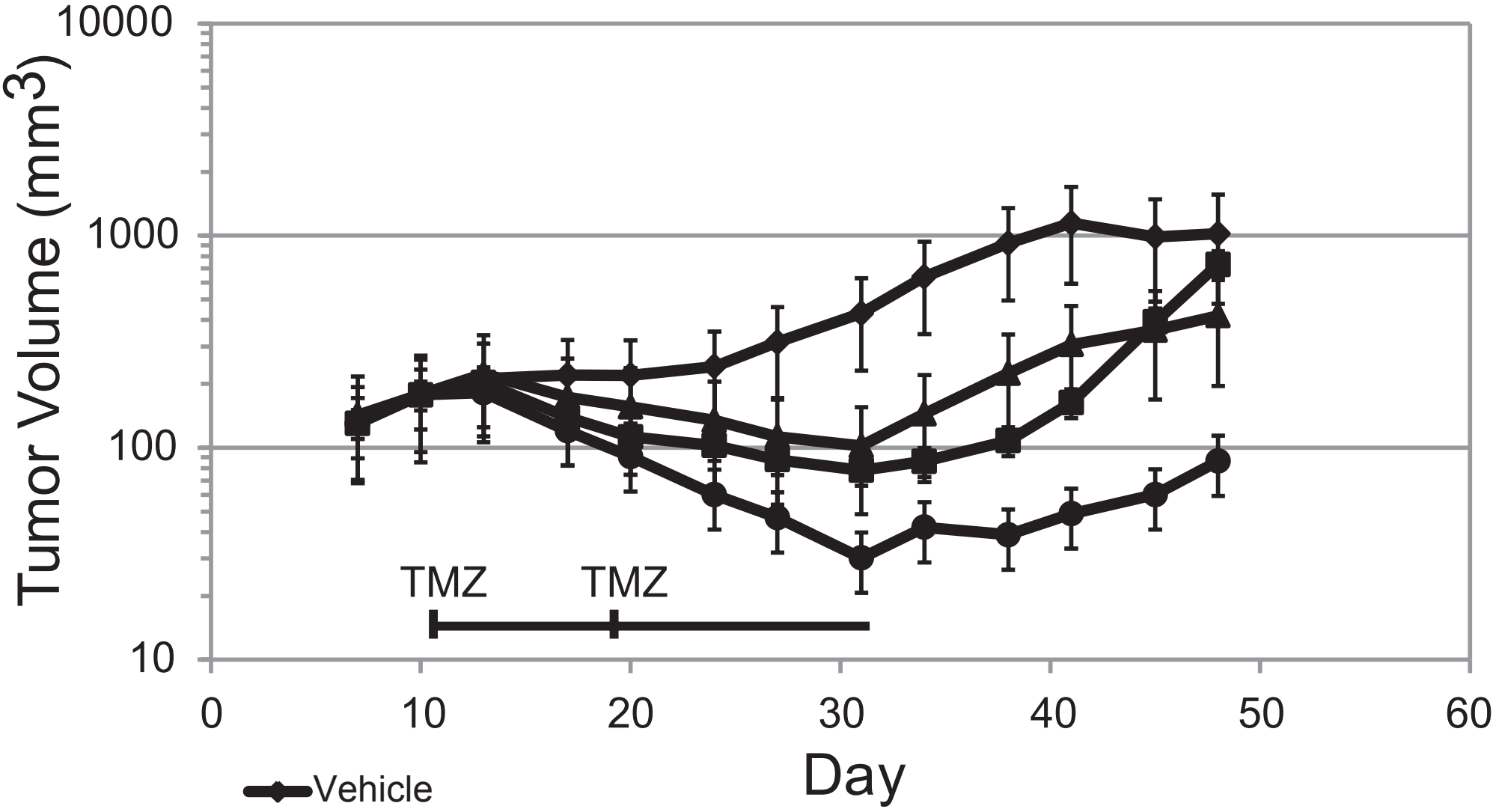
10000
1000
100
10
Tumor Volume (mm3)
TMZ
TMZ
0
10
20
30
40
50
60
Day
Vehicle
Abemaciclib 50 mg/kg PO
TMZ 3 mg/kg IP
Abemaciclib 50 mg/kg PO / TMZ 3 mg/kg IP

Figure 7.

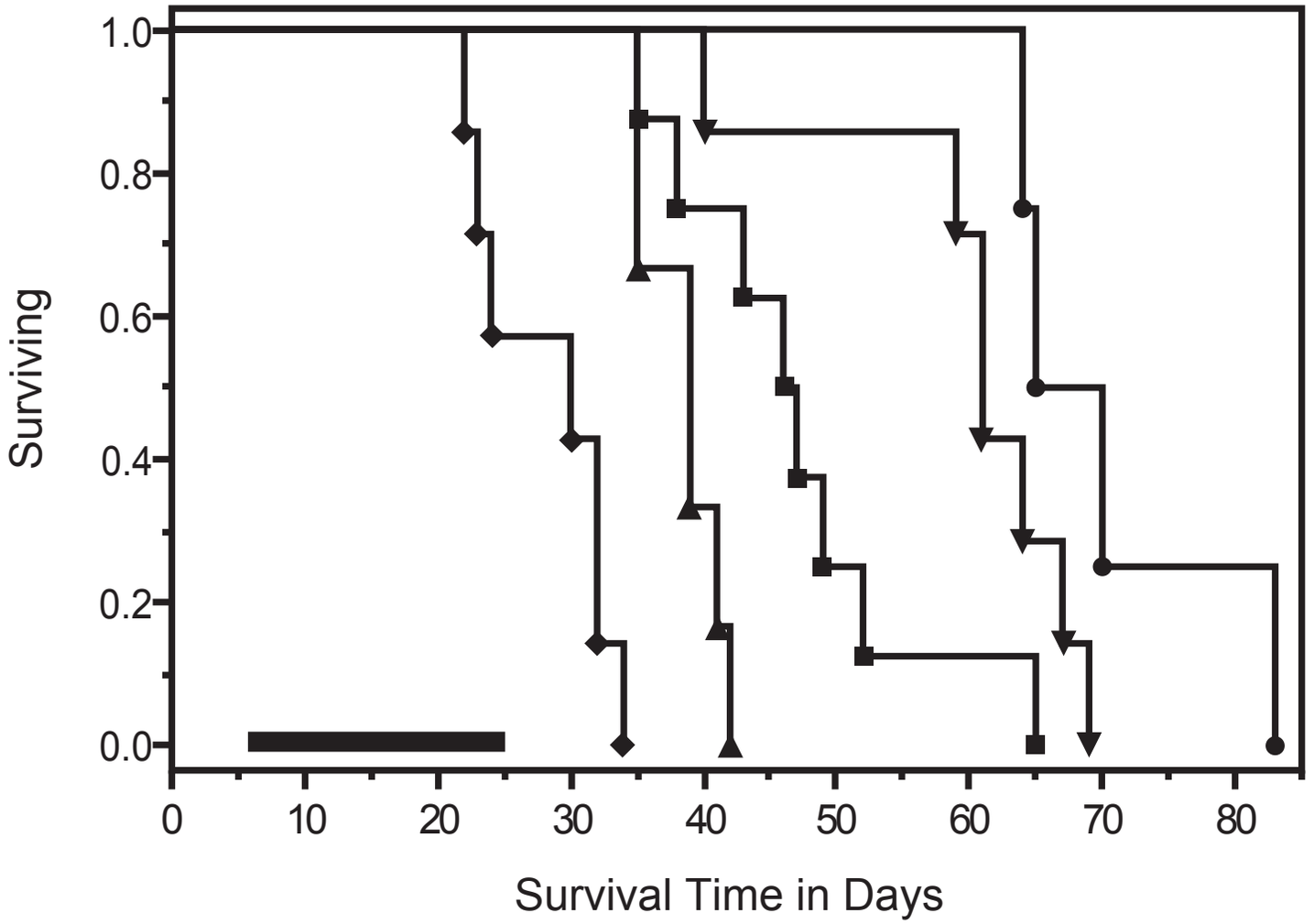

Symbol	Compound (mg/kg)	Group	Dose Route	N	Median (days)	p Value	Increase in Survival vs. Vehicle (days)
◆	None	Vehicle	PO	8	30		—
▲	Abemaciclib (40)	QD x 20	PO	8	39	0.0004	9
■	TMZ (3)	Days 6, 13	IP	8	46.5	<0.0001	16.5
▼	Abemaciclib (40) + TMZ (3)	QD x 20 Days 6, 13	PO IP	8	61	0.0002	31
●	Abemaciclib (40) + TMZ (3)	Q2D x 20 Days 6, 13	PO IP	8	67.5	0.0032	37.5